Chapter 3
Bond Between EBR FRP and Concrete

Claudio Mazzotti, Antonio Bilotta, Christian Carloni, Francesca Ceroni, Tommaso D'Antino, Emidio Nigro and Carlo Pellegrino

Abstract This chapter provides an overview of the debonding process between the FRP reinforcement and the concrete substrate. The main aspects of the debonding phenomenon are described and discussed, showing also mechanical interpretation of different processes. Experimental techniques to study the bond behavior between FRP and concrete are also described and corresponding available experimental results are shown to compare performances of different set-ups. Finally, an extensive description of the existing bond capacity predicting models is reported, together with the main international Codes provisions, allowing the designer for operating in common practice.

Keywords FRP · Strengthening · Bond · Concrete

General Aspects

Mechanism of Debonding Failure

Debonding of FRP reinforcement is one of most important failure modes to be considered in design of strengthening of reinforced concrete structures by means of composite materials (Teng et al. 2001). Following recent design Codes and Recommendations (*fib* 2001; ACI 2008; CNR 2013), anchorage force (bond

C. Mazzotti (✉) · C. Carloni
University of Bologna, Bologna, Italy
e-mail: claudio.mazzotti@unibo.it

A. Bilotta · E. Nigro
University of Naples Federico II, Naples, Italy

F. Ceroni
University of Sannio, Benevento, Italy

T. D'Antino · C. Pellegrino
University of Padua, Padua, Italy

C. Pellegrino and J. Sena-Cruz (eds.), *Design Procedures for the Use of Composites in Strengthening of Reinforced Concrete Structures*, RILEM State-of-the-Art Reports 19, DOI 10.1007/978-94-017-7336-2_3

capacity) of FRP sheets attached to the concrete surface is the basis of design rules for shear strengthening applications, since it determines maximum force that can be applied to external reinforcement. Moreover, intermediate crack-induced debonding (Teng et al. 2003) between concrete and external FRP plate/sheet reinforcement (debonding initiating at flexural cracks along the beam) is the failure mode governing maximum FRP strain which can be adopted for flexural design. For reinforcement with FRP plates, design maximum strain against debonding is usually significantly smaller than corresponding to composite failure.

When strengthening reinforced concrete members with FRP composites, the role of bond between concrete and FRP is of great relevance due to the brittleness of the failure mechanism by debonding (loss of adhesion). According to the capacity design criterion, such a failure mechanism shall occur prior to flexural or shear failure of the strengthened member. The loss of adhesion between FRP and concrete may concern both laminates or sheets applied to reinforced concrete beams as flexural and/or shear strengthening. As shown in Fig. 3.1, debonding may take place within the adhesive, between concrete and adhesive, in concrete itself, or within the FRP reinforcement (e.g. at the interface between two adjacent layers bonded each other) with different fibre inclination angles. When proper installation is performed, because the adhesive strength is typically much higher than the concrete tensile strength, debonding always takes place within the concrete itself with removal of a layer of material, whose thickness may range from few millimeters to the whole concrete cover.

Debonding failure modes for laminates or sheets used for flexural strengthening may be classified in the following four categories (Fig. 3.2):

1. Plate/sheet end debonding
2. Intermediate debonding caused by flexural cracks
3. Debonding caused by diagonal shear cracks
4. Debonding caused by irregularities and unevenness of concrete surface

The first two modes are the most frequent in ordinary situations.

The tension in the plate/sheet is transferred to the concrete mainly by shear stresses in the adhesive. When a limit shear stress (bond strength) is attained,

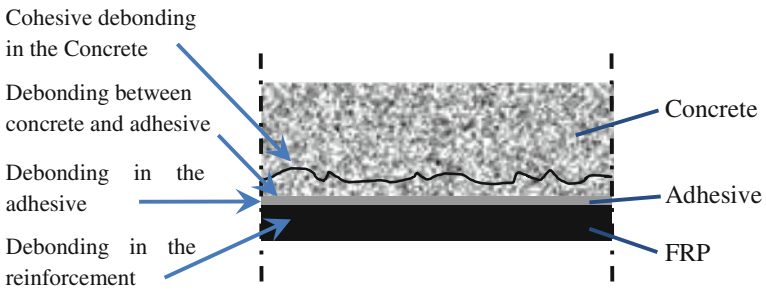

Fig. 3.1 Debonding mechanisms between FRP and concrete

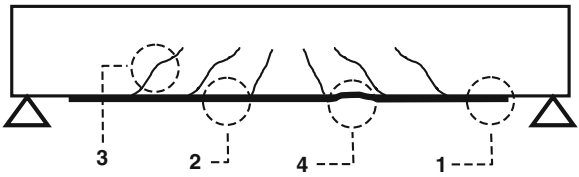

Fig. 3.2 Modes of debonding failure in a beam under flexure and shear

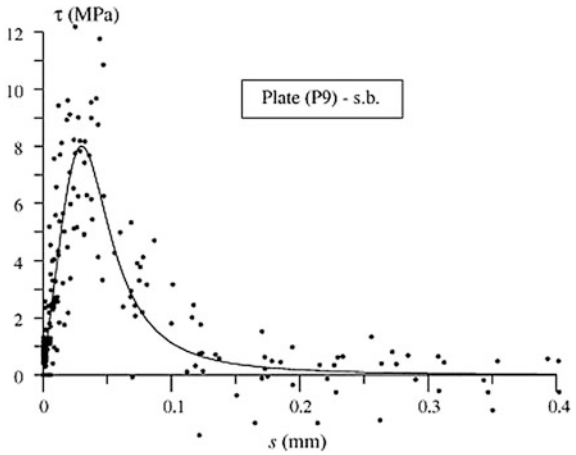

Fig. 3.3 Interface shear stress-slip local behavior

debonding starts according to one of previous modes. During the process, a shifting of the active zone (that able to transfer force) can be observed, which means that only part of the bonded area is effective. That is, as cracking in the concrete propagates, bond resistance is gradually lost in the zone near the load, but in the meantime it is activated farther away from the load. The implication is, then, that the anchorage force cannot increase with an increase in the bond length, and that the ultimate tensile strength of a plate may never be reached, no matter how long the bonded length is. This leads to the important concept of effective bond length, beyond which any increase in the bond length cannot increase the anchorage strength. From a mechanical point of view, it can be explained by considering a local non-linear brittle shear stress-slip relationship showing a post-peak softening behaviour, as confirmed by a number of experimental tests (Fig. 3.3).

Normal stresses in the FRP reinforcement are mainly transmitted through the substrate and the adhesive by means of shear stresses applied to its surface, usually producing Mode II shear condition (Buyukozturk et al. 2004). In fact, only a small layer of concrete close to the interface is subject to very high shear stresses and criterion of the maximum release rate requires that fracture propagates along it. During debonding, the portion of concrete where shear stresses are transmitted is in fact very small: 3–5 cm depth.

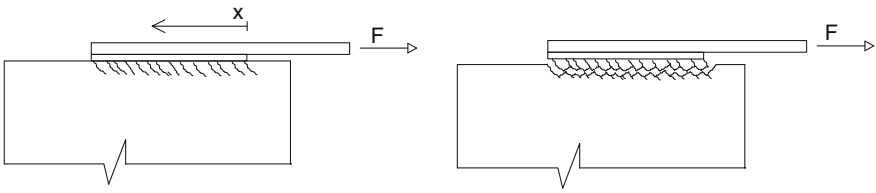

Fig. 3.4 Failure mechanism at the interface level

Failure mechanism, according to Mohr-Coulomb criterion can be described as follow: inclined microcracks start locally in Mode I condition in the small superficial layer of concrete because its tensile strength is much lower than that of the adhesive (see Fig. 3.4). Inclined cracks cannot propagate more than few millimetres inside the concrete specimen because stresses decrease very rapidly with depth from FRP-concrete interface. Then, a series of inclined struts clamped to concrete substrate are subject to compression and bending. Final failure can be due to concrete crushing in compression or transverse cracking on tensile side of concrete struts, depending on dimensions of struts, and a corrugated debonding surface parallel to the interface is typically detected after failure.

When the structural element strengthened with FRP is also subject to flexural or shear deformation (e.g. beams) the effect of the curvature has to be taken into account; it produces an increase of the peeling stresses along the direction orthogonal to the FRP surface, leading to an early detachment when this stress component is not negligible. According to the described mechanisms, the failure mode is sometimes addressed like a mix-mode failure and, for simplicity, it is usually governed by a Mode II fracture energy empirically defined.

Anchorage Length

The formulation suggested by *fib* (2001) and CNR (2004) for the effective bond length is:

$$L_e = \sqrt{\frac{E_f \cdot t_f}{2 \cdot f_{ctm}}} \tag{3.1}$$

whereas the formulation provided by Chen and Teng (2001) is:

$$l_{ed} = \sqrt{\frac{E_f \cdot t_f}{\sqrt{f'_c}}} \tag{3.2}$$

Both relationships show the obvious inverse dependence of l_{ed} on the substrate strength. If a rigid-softening bilinear law is assumed, the following theoretical relationship can be written (Faella et al. 2002):

$$l_e = \frac{\pi}{2}\sqrt{\frac{E_f \cdot t_f}{k_u}} = \frac{\pi}{2}\sqrt{\frac{E_f \cdot t_f}{\tau_{max}/s_u}} \tag{3.3}$$

in which the effective bond length is expressed as function of the stiffness of the substrate. Equation (3.3) can be rewritten as follows:

$$l_e = s_u\sqrt{\frac{\pi^2 \cdot E_f \cdot t_f}{8 \cdot \Gamma_f}} \tag{3.4}$$

This relationship provides mean values of the effective length, if the mean values of fracture energy is used. About the estimation of s_u, in Bilotta et al. (2011) the value 0.25 mm allowed the theoretical distribution of strain along the FRP reinforcement for fitting quite well the experimental ones by means of an inverse analysis procedure (Faella et al. 2009). Under the assumption of bilinear bond law, indeed, the procedure minimizes the scatter between the numerical and the experimental strains as the main parameters of the bond law are changed. However, the numerous experimental results investigated were referred to specimens with concrete compressive strength of about 20 MPa. A wider range of concrete strength should be investigated in order to have a more reliable estimation of s_u. Note that the following expression of s_u (Eq. 3.5) can be deduced by the relationships provided in Lu et al. (2005) under the bilinear bond law hypothesis:

$$s_u = \frac{2 \cdot G_f}{\tau_{max}} = \frac{0.41 \cdot \beta}{f_{ct}^{0.5}} \tag{3.5}$$

being $G_f = 0.308$ N/mm and $\tau_{max} = 1.5$ MPa; β is a shape factor similar to k_b. For $\beta = 1$ and $f_c = 20$ MPa, the value $s_u \approx 0.25$ mm is confirmed.

Figure 3.5 shows the strain profiles recorded during shear tests carried out on two series of three sheets (V18a,V19a and V20a—see Fig. 3.5a) and three plates (laminates) (V1a,V2a and V3a—see Fig. 3.5b) glued on concrete specimens for a length $l_b = 400$ mm (Bilotta 2010). The strain profiles were recorded when the first debonding load, P_{fd}, that identified the beginning of debonding, was attained. Hence the distance from FRP end at which strains equal to zero were recorded represents the experimental effective bond length value, $l_{e,exp}$. The agreement between $l_{e,exp}$ and the value l_e calculated through the formulation (3.4) is good. However, in order to obtain a design value for the effective bond length, the Eq. (3.4) is modified as follows:

$$l_{ed} = \frac{1}{\gamma_{Rd} \cdot \tau_{max}}\sqrt{\frac{\pi^2 \cdot E_f \cdot t_f \cdot \Gamma_{Fd}}{2}} \text{ with } \tau_{max} = \frac{2 \cdot \Gamma_{Fd}}{s_u} \tag{3.6}$$

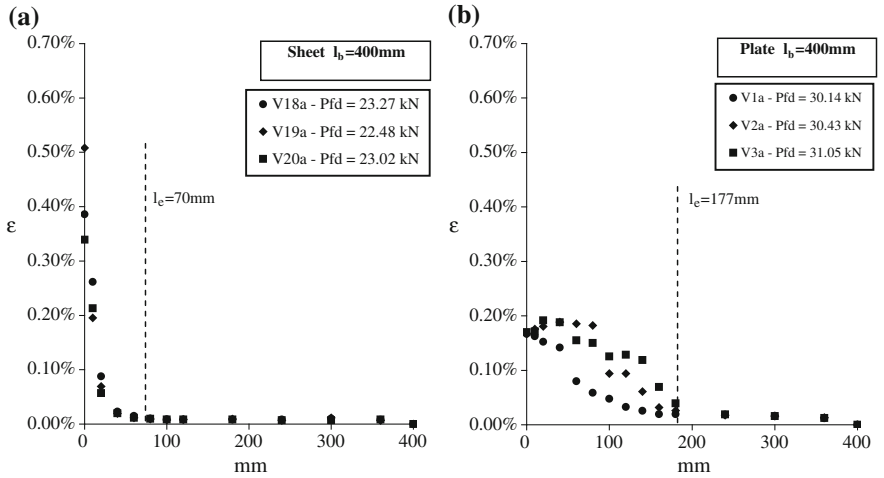

Fig. 3.5 Strain profiles along FRP: **a** sheets; **b** plates

In Eq. (3.6), which is included in CNR (2013), the design value of the fracture energy, Γ_{Fd}, is introduced and $\gamma_{Rd} = 1.25$ is a model factor introduced because it is not currently possible to calibrate a design value for s_u with the available experimental data.

The effective bond length calculated through Eqs. (3.1), (3.2), (3.4) and (3.6) are plotted against the concrete compressive strength, f_{cm}, for sheets ($E_f = 216$ GPa and $t_f = 0.166$ mm) and plates ($E_f = 171$ GPa and $t_f = 1.4$ mm) in Fig. 3.6a, b, respectively.

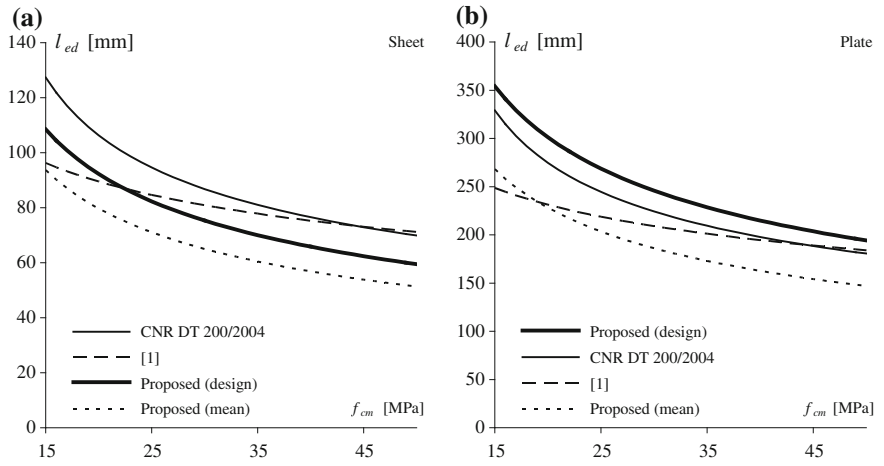

Fig. 3.6 Bond length versus concrete compressive strength: **a** Sheets **b** Plates

The mean values provided by the proposed formulation are lower than provisions given by Chen and Teng (2001) for both sheets and plates, whichever the concrete compressive strength is. On the contrary, the design values are slightly less safe for sheets and slightly more safe for plates.

Effect of Surface Preparation

As well recognized in literature, the bond capacity between the FRP system and the concrete depends on a number of factors, including the material properties of the epoxy matrix and of the fibers as well as the properties of the concrete substrate (Miller and Nanni 1999). Among these, particularly important are the concrete strength and surface roughness and cleanliness. For this reason, the surface preparation methods are a key issue governing the possible success of the strengthening intervention. In more details, surface preparation is the process by which the concrete substrate must be sound, clean, and suitably roughened. This process include the removal of unsound concrete and bond-inhibiting films, strength verification, and opening of the pore structure.

Some of the most common surface preparation methods are: brushing, grinding, scarifying, bush-hammering, steel shotblasting, sandblasting, each with advantages and disadvantages associated to several factors as the desired roughness profile of the prepared surface, cost, and processing time. As a confirmation, Chajes et al. (1996) showed that the interfacial bond strength increased when the surface is prepared using mechanical abrading. Similarly, Yao et al. (2005) presented an experimental study on the bond shear strength between FRP and concrete using a near end supported (NES) single-shear pull test; the corresponding test results emphasized the role of a careful specimen preparation that significantly affected the bond capacity, together with the amount of the removed substrate at failure. Delaney and Karbhari (2007) reported that the surface preparation influences not only the instantaneous behaviour but also the durability of the system. Unfortunately, extensive experimental data concerning the FRP to concrete bond quality are available mainly for sandblasting while for others treatments few data can be found (Mazzotti et al. 2007).

At a design level, most FRP design and construction Guidelines recommend surface preparation methods for effective applications. The International Concrete Repair Institute (ICRI) produced a guideline (Savoia et al. 2009) for concrete surface preparation for polymer overlays that carefully describes several concrete surface preparation methods stating the advantages and the disadvantages of each one. The ACI Committee 440 (2002) suggests abrasive or water blasting techniques for surface preparation to a minimum concrete surface profile CSP 3, as defined by ICRI. Nevertheless, even with roughness level not strictly complying with ICRI/ACI (1999) prescriptions, an adequate level of adhesion can be obtained (Shen et al. 2002). The Italian technical guideline DT 200 (CNR 2004) suggests that once the quality control of the substrate has been performed, the deteriorated

concrete has been removed, the concrete cross-section restored, and the existing steel reinforcement has been properly treated, then sandblasting of the concrete surface to be strengthened should be performed.

Ueda and Dai (2005) observed that a large amount of the scattering of experimental results concerning bond strength is due to concrete surface conditions and preparation, even when different operators or laboratories follow the same surface treatment procedure. More recently Serbescu et al. (2013) collected a large amount of data from which they calibrated some empirical laws also concerning the effect of surface preparation.

In Iovinella et al. (2013) an extensive experimental campaign is described, where surface roughness was measured on concrete specimens treated with different surface preparation, prior to FRP application, by means of a laser profilometer and its various aspects were condensed in a simple roughness coefficient (Fig. 3.7a). Two types of tests were carried out on the strengthened specimens: conventional pull-off tests (suitable for on-site application—Fig. 3.7b) and pull-out bond tests. Results show a clear correlation between the type of surface preparation and the bond strength obtained by pull-out tests (Fig. 3.8a). The interface law (by means of the fracture energy—Fig. 3.8b), which will be introduced in the next section, is also affected by the type and effectiveness of the considered treatment. The quantitative approach allowed for proposing a simple design formula able to take into account the specific roughness considered when predicting the bond strength.

In this framework, by following the CNR (2004) approach the fracture energy can be defined as:

$$\Gamma_f = k_G \cdot k_b \cdot k_r \sqrt{f_{cm} \cdot f_{ctm}} \tag{3.7}$$

where $k_r = 0.766 + 0.08 \cdot I_R$, while all the other coefficients have the conventional meaning.

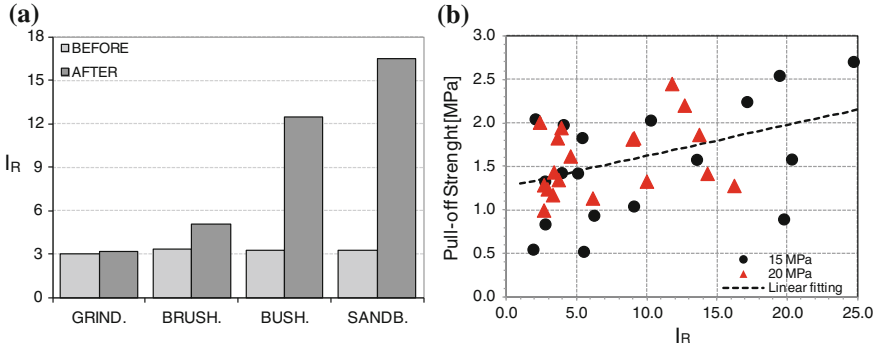

Fig. 3.7 **a** Roughness index measured from different surface preparation and **b** corresponding pull-off strength (Iovinella et al. 2013)

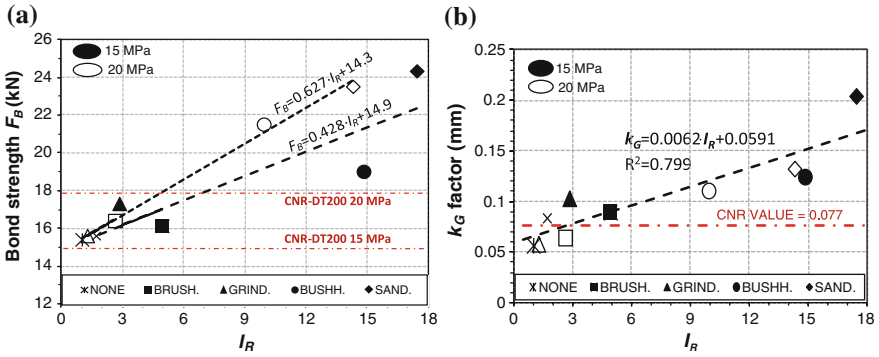

Fig. 3.8 **a** Bond strength and **b** fracture energy coefficient k_G as a function of roughness index (Iovinella et al. 2013)

Bond as a Fracture Mechanics Process

Introduction

Fracture propagation during intermediate crack-induced debonding (ICD) occurs in concrete, therefore it is reasonable to assume that the *quasi-brittle behaviour* of concrete governs the debonding process. It seems appropriate to model the debonding mechanism within the framework of fracture mechanics applied to quasi-brittle materials (Bazant and Planas 1997). In linear elastic fracture mechanics (LEFM) it is well known that a singularity in the stress and displacement fields occurs at the crack tip (Anderson 2004; Bazant and Planas 1997). In LEFM the nonlinearity of the material is neglected although in applications only a limit value of the stress can be reached and in a zone near the crack tip a stress re-distribution occurs, which is related to the nonlinearity of the material. The nonlinearity near the crack tip can be due to hardening or softening of the material. In order to overcome the inapplicability of LEFM for quasi-brittle materials such as concrete, the concept of *fracture process zone* (FPZ) is introduced. The FPZ represents a bridging zone between the cracked and uncracked regions, where progressive softening occurs. It is important to point out that in quasi-brittle materials the FPZ is most likely coincident with, or close in size to, the region of material nonlinearity. In other materials, such as steel, the softening part of the nonlinear zone is negligible and the nonlinear hardening zone is predominant. The characteristics and size of the FPZ depend on the material. In concrete, the FPZ is related to progressive damage that is associated with several complex phenomena (microcracking, void formation, etc.). As the fracture process progresses in concrete, coalescence of microcracks in the FPZ gives continuity to the already existing crack and consequently the crack propagates.

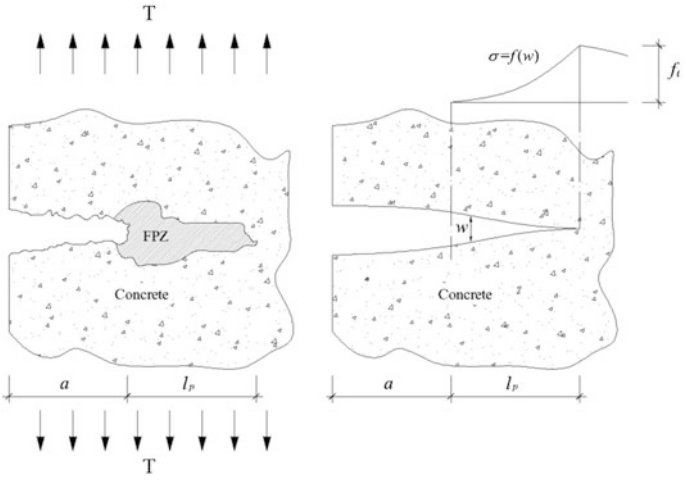

Fig. 3.9 Fracture process zone in concrete and cohesive crack model

The concept of cohesive zone or cohesive crack is associated with the work of Hillerborg et al. (1976). The cohesive crack model is a simple model for the FPZ in concrete and can be taken as a reference to compare other models (Elices et al. 2002). For a Mode-I condition, it is assumed that within the FPZ a crack tip should not be defined. Conversely, the stress σ transferred through the cohesive crack is a function of the crack opening w (Fig. 3.9). The function $\sigma = f(w)$ is characteristic of the material and is often called the *softening function*. When $w = 0$, $\sigma = f_t$, which is the tensile strength of concrete.

Several researchers attempted to study ICD phenomenon and the debonding in direct-shear tests as a Mode-II fracture problem (Anderson 2004) where the interface region is idealized to be of zero thickness with well-defined material properties (Ali-Ahmad et al. 2006; Wu and Niu 2007; Mazzotti et al. 2008). In this idealization, the interfacial crack, associated with initiation and propagation of debonding, is subject to a Mode-II loading condition. The quasi-brittle behaviour of the interfacial crack, in the spirit of the cohesive crack model, is described by introducing a cohesive material law, which relates the interface shear stress (τ) to the relative slip (s) between FRP and concrete. It is important to highlight that the cohesive material law τ-s represents the constitutive law of a fictitious material that links the FRP strip to the concrete substrate (interface). The shear stress should not be associated with the shear stress that occurs in concrete at a particular distance from the concrete surface. Although it is reasonable to assume that the stress field in concrete near the interface has an important role in the stress transfer and therefore in the debonding mechanism, the cohesive material law, herein introduced, aims to describe the interfacial debonding at the macro-scale; hence its parameters should not refer to the actual stress state in concrete at the microscopic level.

Fracture along the interface does not occur on an ideal plane parallel to the FRP strip but follows a tortuous path, which is in part controlled by the distribution of the aggregates and in part by the mixed-mode nature of the fracture process at the microscopic level. In fact, the crack continuously kinks to follow the path that requires the least amount of energy and is related to the fracture properties of the two materials (Hutchinson and Suo 1992; Gunes 2004; Gunes et al. 2009). At the macroscopic level, the microscopic mixed-mode fracture can be considered a Mode-II fracture at the FRP-concrete interface.

Direct-Shear Tests

Several analytical/numerical procedures to estimate the cohesive interfacial behaviour from the load response of direct-shear tests were developed. For example, Ali-Ahmad et al. (2006) established an experimental procedure to directly determine the Mode-II interfacial fracture law using DIC measurements. The cohesive material law for the interface, when implemented in a numerical analysis procedure, allowed for predicting the load response of concrete beams strengthened with externally-bonded FRP sheets (Wu and Yin 2003; Ali-Ahmad et al. 2007; Wu and Niu 2007). Among others, Ferracuti et al. (2006, 2007); Mazzotti et al. (2008), and Carrara et al. (2011) used a procedure similar to Ali-Ahmad et al. (2006). In those studies, the authors used strain gauge readings along the FRP surface to obtain the interfacial law. Pellegrino et al. (2008) and Pellegrino and Modena (2009) used a double-lap shear test and a small-beam test to investigate the effect of the axial stiffness of the composite on the cohesive material law and indicated the need of more research to study this aspect.

In what follows, reference will be made to the experimental work reported in Subramaniam et al. (2007). Single-lap direct-shear tests were used to evaluate the FRP-concrete debonding using the classical pull-push configuration. The tensile load was applied to the FRP sheet, while the concrete block was restrained against movement. This set-up is also referred to as the *near-end supported single-shear test* (Yao et al. 2005).

Figure 3.10 shows the specimen dimensions and the loading arrangement (Carloni and Subramaniam 2012). The Cartesian system depicted in Fig. 3.2 will be used as a reference system for the strain analysis and fracture mechanics approach that follow. Details of the test set-up and materials used can be found in Subramaniam et al. (2007, 2011). Two LVDTs were mounted on the concrete surface close to the edge of the bonded area. The LVDTs reacted off of a thin aluminium Ω-shaped plate, which was glued to the FRP surface at the beginning of the bonded area as shown in Fig. 3.10. The average of the two LVDT readings was named *global slip*. Tests were conducted in displacement control by increasing the global slip at a constant rate equal to 0.00065 mm/s, up to failure. The modality of failure of all direct-shear test specimens was associated with progressive debonding of the FRP sheet from the concrete substrate.

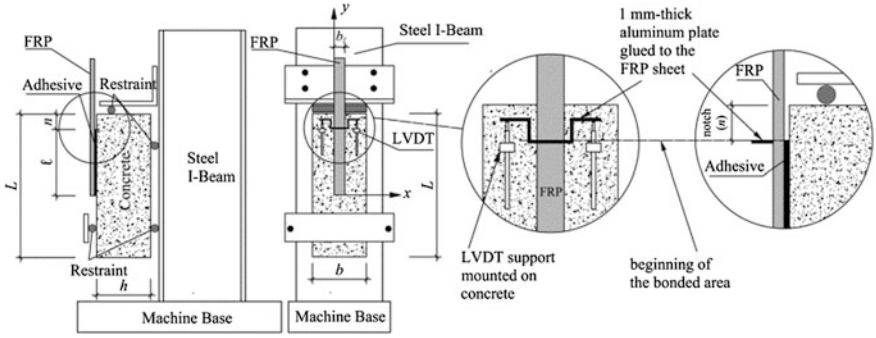

Fig. 3.10 Specimen dimensions and loading arrangement (Subramaniam et al. 2007)

The strain components on the surface of the FRP and surrounding concrete during the monotonic quasi-static tests were determined from the displacement field, which was measured using a full-field optical technique known as digital image correlation (DIC). Details about DIC can be found in Sutton et al. (1983, 2009).

The typical load-global slip response, which can be found in the aforementioned publications, showed an initial linear ascending region followed by a non-linear response. The end of the non-linear part of the response was typically marked a by a load drop that indicated that the interfacial crack has formed. The load was nominally constant after the load drop and the value of the constant load is termed *load-carrying capacity* or *bond capacity* and indicated as P_{crit}. An example of the load response, which corresponds to test W_7 in Subramaniam et al. (2007), is depicted in Fig. 3.11.

Figure 3.12 shows the variation of the axial strain ε_{yy} on the surface of the FRP along the bonded length for three points (A, B, and C) of the load response of Fig. 3.11 in the region where the load is nominally constant. The axial strain distribution along the FRP obtained from all specimens tested was nominally similar. The experimental strain values are represented by markers. The axial strain values were determined along the center line of the FRP sheet by averaging the strain across a 10 mm-wide strip for each value of y. The experimental nonlinear strain distribution along the bonded length of Fig. 3.12 was approximated using the following expression (solid line in Fig. 3.12):

$$\varepsilon_{yy} = \varepsilon_0 + \frac{\alpha}{1 + e^{-\frac{y-y_0}{\beta}}} \tag{3.8}$$

where α, β, y_0, and ε_0 were determined using nonlinear regression analysis of the strains obtained from DIC. The choice of the Eq. (3.8) is not unique (Dai et al. 2005a, b, 2006; Zhou et al. 2010; Liu and Wu 2012). The observed strain distribution along the FRP was essentially equal to zero close to the unloaded end. There was a rapid increase in strain upon approaching the loaded end. The strain leveled

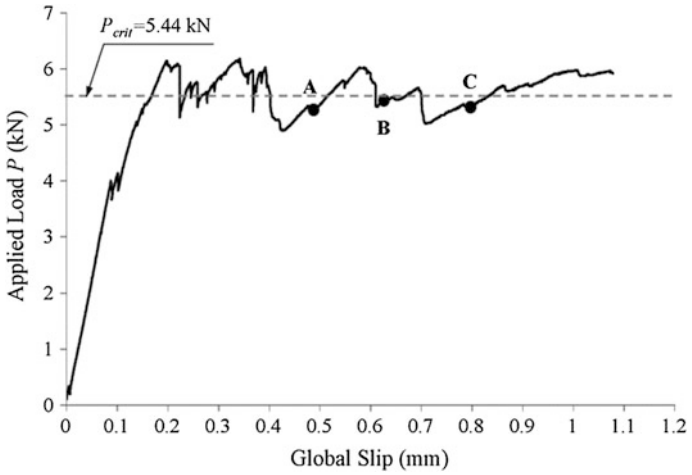

Fig. 3.11 Typical load respond (Test W_7) of a direct shear test (Subramaniam et al. 2007)

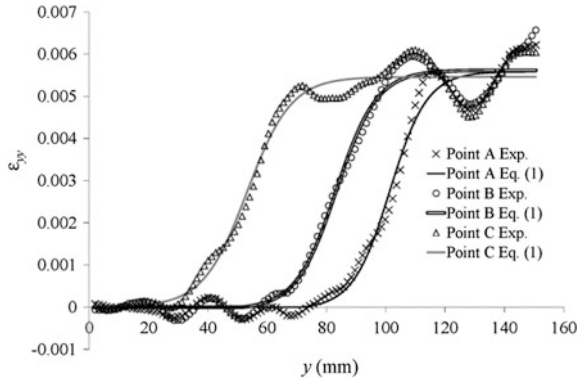

Fig. 3.12 Axial strain profiles corresponding to three points (A, B, and C) of the load response of Fig. 3.11

off at a value $\bar{\varepsilon}_{yy}$ which was approximately equal to 5580 με for point A. The observed strain distribution was divided into three main regions: (a) the stress-free zone (SFZ); (b) the stress-transfer zone (STZ); and (c) the fully-debonded zone (FDZ). In the FDZ, the strains were essentially constant and were found to remain unchanged with increasing the global slip, which is consistent with the observation that the load remained nominally constant (P_{crit}) after the debonding process propagated. It can be observed that a simple translation of the STZ further along the length of the FRP sheet occurred as the global slip increased while its shape remained constant. The translation of the STZ indicates self-similar crack growth. It should be noticed that the STZ does not correspond to the FPZ.

The progressive debonding of the FRP composite sheet from concrete is associated with a STZ of a fixed length L_{STZ}, which translates as the crack advances (Fig. 3.11). L_{STZ} is also termed the *effective bond length* (Chen and Teng 2001) or

Table 3.1 Fracture parameters of the tests published in Subramaniam et al. (2007)

Test	b_f (mm)	P_{crit} (kN)	L_{STZ} (mm)	ε_{yy} (με)	G_F (MPa × mm)
W_1	46	12.90	80	7200	0.874
W_2	46	12.05	76	6200	0.634
W_3	46	13.20	75	5900	0.563
W_4	38	10.09	81	6400	0.692
W_5	38	10.02	73	6200	0.652
W_6	25	5.54	80	5600	0.546
W_7	25	5.44	76	5600	0.530
W_8	25	5.36	69	6400	0.705
W_9	19	4.27	75	6400	0.686
W_10	19	4.05	78	5900	0.579

the *development length* (ACI 440.2R-08 2008). The average values of L_{STZ} are plotted in Subramaniam et al. (2007) and summarized in Table 3.1 together with the other fracture parameters, the maximum strain $\bar{\varepsilon}_{yy}$, and the load-carrying capacity.

Cohesive Material Law

From the measured strain ε_{yy} along the bonded length, the equilibrium of an infinitesimal segment of the composite strip yields (Taljsten 1996, 1997a, b):

$$\tau_{zy} = E_f t_f \frac{d\varepsilon_{yy}}{dy} \tag{3.9}$$

E_f and t_f are the elastic modulus and thickness of the composite, respectively. The following assumptions were made: (a) the FRP sheet was homogenous and linear elastic; (b) the thickness and the width of the FRP sheet were constant along the bonded length; (c) the interface was only subject to shear loading; (d) the interface between the FRP and the concrete was assumed to be of infinitesimal thickness; and (e) the concrete substrate was rigid.

The relative slip, $s(y)$, between FRP and concrete at a given location on the FRP was obtained by integrating the axial strain in the FRP up to that point.

Lu et al. (2005) commented on the possible ways to obtain the τ–s curves, observing that the violent local variations of strain measured by strain gauges entailed for substantial differences in the fracture parameters. The procedure followed by Subramaniam et al. (2007, 2011) used the strain contours obtained from DIC, which allowed to identify the fluctuations of the strain profile due to the local variations of the FRP and the substrate (Ali-Ahmad et al. 2006). The cohesive material law curves corresponding to points A, B, and C of the load response of Fig. 3.11 are shown in Fig. 3.13.

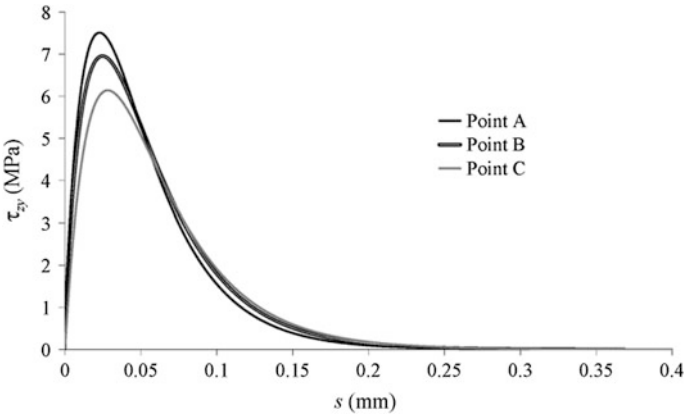

Fig. 3.13 τ_{zy} –s curves for points A, B, and C in Fig. 3.3

Several expressions of the cohesive material law are available in the literature. For example, Ferracuti et al. (2006, 2007) proposed the following relationship:

$$\tau_{zy}(s) = \bar{\tau}\frac{s}{\bar{s}}\frac{n}{(n-1)+\left(\frac{s}{\bar{s}}\right)^n} \tag{3.10}$$

where $\bar{\tau}$ the maximum is shear stress and $\bar{s}$ is the corresponding slip. Other researchers indicated these parameters as τ_{max} and s_0, respectively. The parameter n (>2) mainly governs the softening branch of the softening curve.

Wu et al. (2012) proposed the following form of the cohesive material law (Liu and Wu 2012):

$$s'' = \frac{\alpha}{\beta}e^{-s/\alpha}\left(1 - e^{-s/\alpha}\right) \tag{3.11}$$

where s'' is the second order derivative of the slip s and is related to the shear stress if the hypotheses introduced above hold. Wu et al. (2012) used an equilibrium approach and compared the results with empirical formulas to identify the parameters α and β.

Interfacial Fracture Energy

The interfacial fracture energy G_F is the energy required to create and fully break the elementary unit area of the cohesive crack. G_F corresponds to the area under the entire τ_{zy}–s curve (Bazant and Planas 1997):

$$G_F = \int_0^{s_f} \tau_{zy}(s)ds. \tag{3.12}$$

where s_f is the slip corresponding to complete separation of the interface. The mean values of G_F for all tests can be found in the published paper (Subramaniam et al. 2007). The mean values of G_F, as well as those for the effective bond length and the maximum strain at debonding $\bar{\varepsilon}_{yy}$, were obtained from ten points of the load response within the range of global slip in which the load was nominally constant.

The relationship between the interfacial fracture energy and the fracture energy of concrete (Mode-I) is still an open discussion among researchers (Achintha and Burgoyne 2008, 2011; Carrara et al. 2011). Although the fracture process in ICD occurs in concrete, it propagates in a mortar-rich thin layer (Carloni and Subramaniam 2010) in which the mechanical and fracture properties are not easily defined. Undoubtedly, the two fracture energies are related although a convincing relationship has not been found yet. Rabinovitch (2004) successfully used the Mode-I fracture energy of concrete to study the end plate debonding (ACI 440.2R-08 2008) using the fracture mechanics concept of energy release rate. In the context of end plate debonding, the energy required to create and fully break the elementary unit area of cohesive crack should be closely related to the fracture energy of concrete as the debonding typically occurs in the concrete cover and peeling stresses are not negligible.

Taljsten (1996) obtained a relationship between the fracture energy and the load-carrying capacity in direct shear tests by considering the energy release during the advancement of the interfacial crack a by an amount da (Fig. 3.14). The *energy release rate* G per unit width b_f of the composite is obtained as:

$$G = \frac{1}{b_f}\left[\frac{\mathrm{d}}{\mathrm{d}a}(F - U_e)\right] \tag{3.13}$$

where F is the work done by the external load and is U_e the elastic energy. When debonding propagates $G = G_F$. If δ is the displacement of the point of application of the applied force P (Fig. 3.14) and C is the compliance of the system, then:

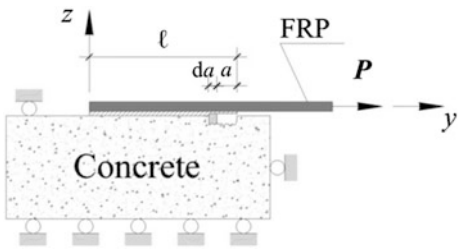

Fig. 3.14 Crack propagation in direct shear tests

$$U_e = \frac{1}{2}P^2 C \tag{3.14}$$

and when the interfacial crack propagates:

$$G_F = \frac{1}{b_f}\left[P\frac{\mathrm{d}\delta}{\mathrm{d}a} - \frac{\mathrm{d}U_e}{\mathrm{d}a}\right] = \frac{1}{b_f}\frac{P^2}{2}\frac{\partial C}{\partial a} \tag{3.15}$$

Therefore:

$$P = \sqrt{2G_F b_f \Big/ \frac{\partial C}{\partial a}} \tag{3.16}$$

If the substrate is considered rigid and the adhesive layer is idealized as a zero-thickness layer:

$$\frac{\partial C}{\partial a} = \frac{1}{E_f b_f t_f} \tag{3.17}$$

where E_f and t_f are the elastic modulus and thickness of the composite, respectively. From Eqs. (3.16) and (3.17), the interface fracture energy G_F is related to the load-carrying capacity (Hearing 2000; Yuan et al. 2001; Liu and Wu 2012; Wu et al. 2002, 2012):

$$P_u = b_f\sqrt{2G_F E_f t_f} \tag{3.18}$$

Equation (3.18) can be obtained through an energy balance approach (Taljsten 1996; Hearing 2000; Focacci et al. 2000; Liu and Wu 2012) and is based on the assumption that a pure Mode-II interfacial crack propagation occurs across the entire width of the composite. The theoretical load-carrying capacity under pure Mode-II was indicated as P_u in Eq. (3.18) to distinguish it from the experimental value P_{crit}.

Concluding Remarks

Contradictory resul ts (Chen and Teng 2001; Subramaniam et al. 2007; Mazzotti et al. 2008; Carloni and Subramaniam 2012) complicate the interpretation of the interfacial fracture energy G_F as a true fracture parameter. The discussion on the nature of the interfacial fracture energy as a true fracture parameter in part arises

from the misuse of Eq. (3.18). From Eq. (3.18), researchers used the experimental load-carrying capacity P_{crit} to determine the fracture energy by assuming that $P_u = P_{crit}$:

$$G_F = \frac{P_{crit}^2}{2b_f^2 E_f t_f} \tag{3.19}$$

This approach led to an erroneous evaluation of G_F because the experimental value of the load-carrying capacity includes the width effect. The fracture energy cannot be directly related to the experimental load-carrying capacity of the interface. The values of G_F determined via Eq. (3.19) scale with the width of the FRP sheet. Hence, the experimental values of the fracture energy determined through Eq. (3.18) should not be considered as *true* values.

In addition to the discussion regarding the purported nature of the fracture energy, concerns remain on the applicability of the direct-shear test results to describe ICD, mainly because of the presence of a Mode-I component (peeling stresses). The Mode-I should not be confused with the one observed above at the microscopic level, but in the spirit of the macroscopic approach of the fictitious interface. The Mode-I opening is described by the relationship between the normal stress (peeling) σ_{zz} and the opening of the crack δ (Martinelli et al. 2011; Carrara and Ferretti 2013). The Mode-I interfacial fracture energy, corresponding to the area of the $\sigma_{zz} - \delta$ curve, is considerably lower than the Mode-II fracture energy (Taljsten 1996; Gunes 2004), thus even a small component of the load perpendicular to the FRP sheet could potentially reduce the load-carrying capacity of the interface. A Mode-I component is always present in the direct-shear test measurements due to the relationship between shear and moment. A limited number of experimental works reported the study of the Mode-I and mixed-mode debonding (Wan et al. 2004; Davalos et al. 2006; Alam et al. 2012). Some authors (Yao et al. 2005) recognized that the effect of a small loading angle (offset) was insignificant for relatively long bonded lengths. The presence of a Mode-I condition in beams can be explained by considering the opening of a flexural/shear crack as illustrated in Fig. 3.15 (Garden and Hollaway 1998). As the crack opens, the two faces of the crack will undergo a relative vertical displacement that will cause a mixed-mode condition for the FRP-concrete interface. Rabinovitch (2008, 2012) used a fracture mechanics approach that considered the Mode-I and Mode-II cohesive material laws and their coupling. A set of nonlinear differential equations was derived by considering a multi-layer description of the strengthened beam. A different length of the STZ for Mode-I and Mode-II can be observed in these studies. Mazzucco et al. (2012) used a similar approach to capture the coupling of the shear and pealing stresses, but introduced a contact-damage model for the adhesion between layers. Gunes et al. (2009) reported that if the strengthened beam was sufficiently strong in shear, the flexural/shear crack mouth displacement would be limited and consequently the mixed-mode nature of debonding fracture would quickly merge

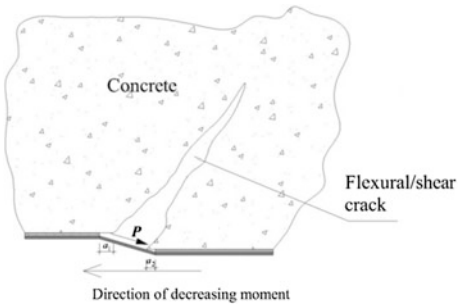

Fig. 3.15 Mixed-mode debonding propagation in beams

into a Mode-II condition. It is interesting to notice that the results published by Alam et al. (2012) showed that the effective bond length increases if the Mode-I component is significant.

Alternative approaches within the framework of fracture mechanics are available in the literature. Achintha and Burgoyne (2008, 2011), for example, studied the debonding phenomenon as a Mode-I problem by considering that the debonding often occurs in the concrete just above the interface. The Mode-I fracture energy of concrete was used in their approach. The authors observed that none of the existing studies available in the literature provided a reliable estimate of the interfacial fracture energy G_F. Gunes et al. (2009) proposed a global energy balance model to predict FRP debonding failure. The amount of energy dissipated in the system during debonding was determined by calculating the change in the potential energy of the system. The component of the energy dissipation due to the debonding process was calculated by means of the interfacial fracture energy.

Cyclic Loads

As shown in previous sections, several theoretical contributions have been proposed by researchers in recent years concerning both the behaviour of the FRP-to-concrete interface and the evaluation of the interface stresses (Ueda and Dai 2005; Dai et al. 2005a). Moreover, many experimental tests have been carried out to evaluate the bond capacity and the effective bond length (Chajes et al. 1996; Bizindavyi et al. 1999; Brosens et al. 2001; Yao et al. 2005). In particular, the influence of FRP stiffness, width, and bond length as well as concrete compressive strength and surface treatments has been investigated in depth (Brosens et al. 2001; De Lorenzis et al. 2001; Savoia et al. 2003; Guo et al. 2005; Lu et al. 2005; Faella et al. 2007a; Nigro et al. 2008). Both theoretical and experimental contributions have led to the development of design guidelines and codes (ACI 440.2R-08 2008; CNR-DT 200 2004; fib bulletin 14 2001). Such guidelines are mainly based on the results of monotonic bond tests, while many strengthened structures are subjected to fatigue loads (i.e. roads and railways bridges) or to shorter but more intense cyclic

actions such as earthquakes. In particular, in these cases the FRP-concrete interface is subject to cyclic stresses which could lead to premature debonding failure.

Thus some researchers have recently begun to investigate the fatigue performance of the FRP-concrete interface (Kobayashi et al. 2003; Dai et al. 2005a, b; Bizindavyi et al. 2003; Diab et al. 2007). Nevertheless, at present, bond tests under cyclic actions performed on CFRP sheets applied on concrete blocks are not as numerous as monotonic tests, and very few contributions are available on cyclic tests performed on CFRP plates. Furthermore, few studies are available on debonding phenomena under few cycles at very high force levels, as typical occurs during earthquakes. During earthquakes, FRP instability in compression may start before debonding; however in some cases (i.e. statically determinate bridge beams and slabs), FRP laminates may be always in tension. Ko and Sato (2007) showed that the load-displacement curves recorded during cyclic tests basically traced the load-displacement curves related to monotonic counterpart tests even if plastic displacements and stiffness reduction were observed due to the partial debonding imposed by the repeated unload/reload cycles. Finally, they showed that partial debonding under cyclic loads does not affect the FRP reinforcement debonding force if adequate bond length is provided.

Compared with monotonic tests, there have been few bond tests under cyclic actions performed on CFRP sheets applied on concrete blocks. Very few contributions are available on cyclic tests performed on CFRP plates and on debonding phenomena under few cycles at high force levels, which typically occur during earthquakes. Therefore, a further series of cyclic Single Shear Tests (SSTs) bond tests under both monotonic and cyclic actions, without inversion of action sign, were performed by Nigro et al. (2011) in order to analyze both the influence of different load paths (few cycles, typical of seismic actions) and the effect of FRP bond lengths on bond behaviour between FRP reinforcement and the concrete substrate. In particular, concrete mix design was specifically designed to obtain low compressive concrete strength, to better simulate the FRP application on existing structural members that need to be strengthened (f_{cm} = 22.5 MPa), whereas sheets and plates were specifically selected to investigate the performance of reinforcements with a low or high value of axial stiffness. Moreover, to investigate the influence of the reinforcement bond length, l_b, on the interface behaviour under cyclic actions, different l_b values were assumed in the experimental program (see Fig. 3.16). Finally, different cyclic load paths were adopted to simulate a seismic event (low number of cycles) of different intensity and to evaluate the extent of the influence of cycle number on bond behaviour.

If $P_{max,M}$ is the maximum debonding load recorded during the monotonic test, the experimental outcomes of cyclic tests showed that the influence of few load-unload cycles up to 70 % of $P_{max,M}$ was negligible in terms of bond stiffness and strength for CFRP sheets both for higher and lower bond lengths than theoretical effective ones); similar results were obtained for plates, even if experimental effective bond lengths were significantly lower than theoretical ones. Moreover, a small number of load-unload cycles (i.e. a total of 40 cycles) up to 90 % of $P_{max,M}$ induced a translation of the shear stress transfer zone along the reinforcement with a

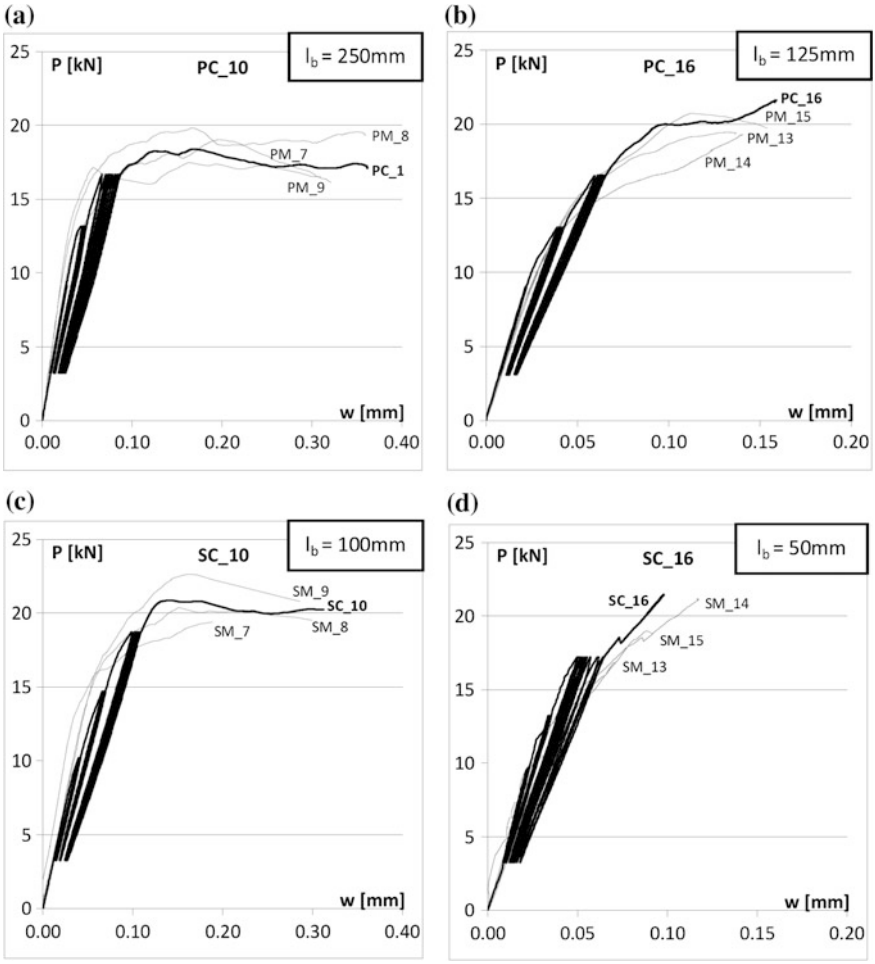

Fig. 3.16 Experimental load-displacement relationships: Plates **a** $l_b = 250$ mm, **b** $l_b = 125$ mm and Sheets, **c** $l_b = 100$ mm, **d** $l_b = 50$ mm

reduction in peak values due to interface damage; however, this phenomenon did not substantially affect debonding loads in the case of bond lengths exceeding the effective bond length. Finally, experimental tests showed that the reduction in bond length up to about 50 % of the theoretical effective bond length induced a comparable reduction in maximum debonding load on specimens subjected to monotonic or cyclic action.

Experimental Analysis of Debonding

Existing Experimental Set-Ups

Several experimental set-ups have been proposed and carried out by researchers in last years to perform bond tests, but a standard procedure has not been defined yet. The following classification of test procedure for bond test is generally assumed (Horiguchi and Saeki 1997; Chen and Teng 2003; Yao et al. 2005, Fig. 3.17): (a) double-shear pull tests; (b) double-shear push tests; (c) single-shear pull tests; (d) single-shear push tests; (e) beam (or bending) tests. These definitions are based on the loading condition in the concrete block and on the symmetry of the specimens (single or double tests refer to the presence of one or two sides of the block strengthened with the FRP reinforcement).

In the cases (a) and (c) the tensile load is applied to the external reinforcement and to the concrete element too (Fig. 3.17a, c); by contrast, in cases (b) and (d) a tensile load is applied to the FRP reinforcement and a pushing action is applied to the concrete block that, thus, is partially compressed (Fig. 3.17b, d). For both set-ups the configuration can be either symmetrical (cases a and b) or asymmetrical (cases c and d).

In the case of beam tests (Fig. 3.17e) the FRP reinforcement is not directly loaded but is however subjected to tensile stresses due to the bending action applied to the concrete element.

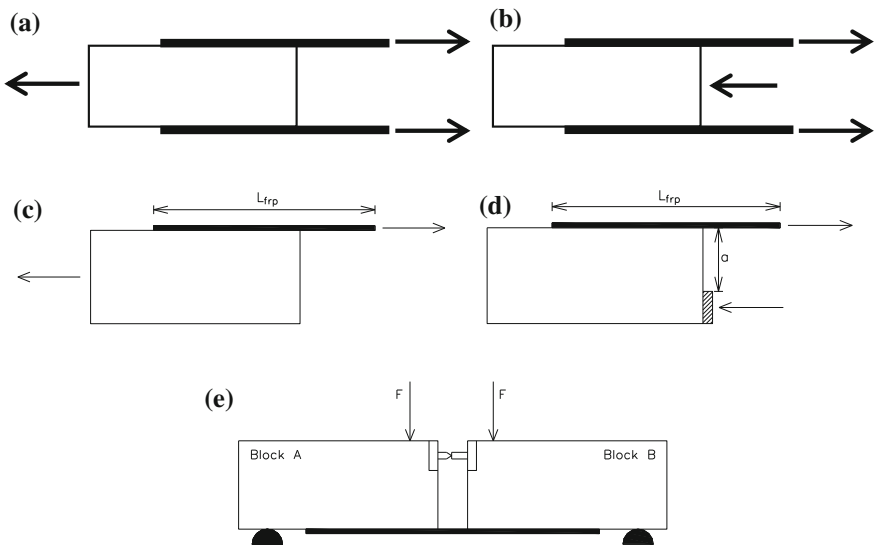

Fig. 3.17 Different set-ups for bond tests on concrete elements externally bonded with FRP materials: **a** double-shear pull test; **b** double-shear push test; **c** single-shear pull test; **d** single-shear push test; **e** beam test

The pull shear test (single or double) corresponds to a loading condition very similar to the actual one, because in existing RC elements the external FRP reinforcement is usually applied on the tension side. However, this scheme is more difficult to realize experimentally compared to the push shear test because the concrete block has to be loaded in tension. Such a loading condition is usually realized by applying tension to steel bars embedded in the block (Brosens and van Gemert 1997; Maeda et al. 1997; Ueda et al. 1999; Wu et al. 2001; Bilotta et al. 2011, Fig. 3.18a). In this scheme the set-up can be more sensitive to the geometrical inaccuracies and imperfections and thus, the repeatability or the variability of the results can be increased.

By contrast, the push shear test is more simple to realize and can give reliable predictions of bond strength, if the compressed area of concrete is not very extended (large value of the distance a in Fig. 3.17d). Indeed, suitable values of this area ensure the development of a bond failure at the concrete-FRP interface, similarly to what occurs in the pull shear test. If the loaded area of concrete is too extended the compressive stresses induced by the pushing force can limit the volume of concrete involved in the failure mechanism and, thus, lower values of debonding load can be attained due to the reduction of the fracture energy.

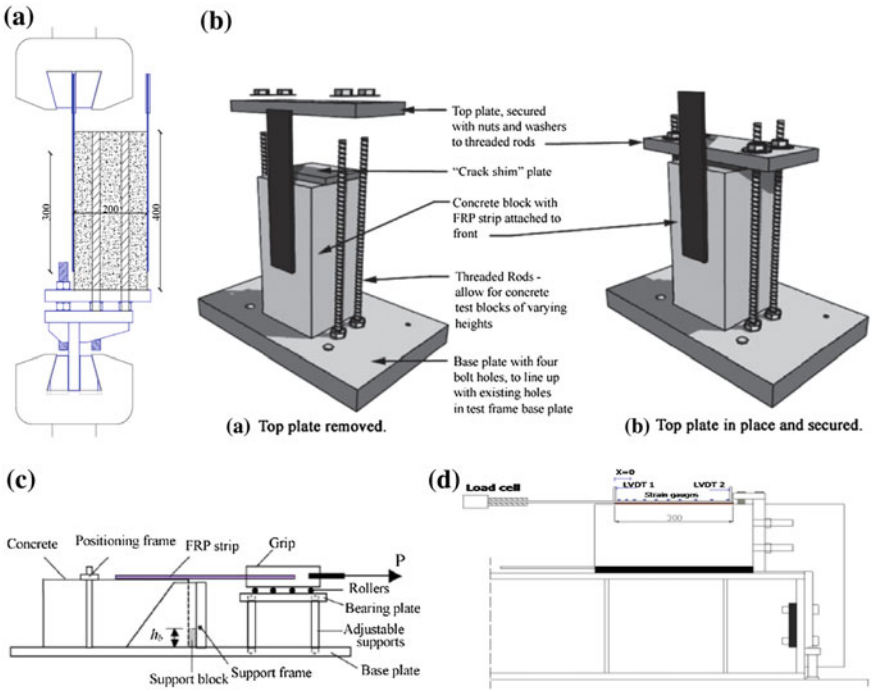

Fig. 3.18 **a** Single pull shear test by (Bilotta et al. 2011a, b); **b** Single push shear test—vertical scheme by (McSweeney and Lopez 2005); **c** Single push shear test—horizontal scheme by (Yao et al. 2005); **d** Single push shear test—horizontal scheme by (Mazzotti et al. 2005)

In general, special attention is required when a symmetrical scheme is realized and the FRP reinforcement is applied on both sides of the concrete specimen (Ceroni and Pecce 2002; Blontrock et al. 2002; Brosen and van Gemert 1997; Guadagnini et al. 2012). The most important problem to solve in this case is the alignment of the two concrete blocks for gripping the FRP reinforcement in the testing machine; indeed, some imperfections can cause additional flexural and torsional stresses in the reinforcement and, thus, can reduce the debonding load. Moreover, in the double-shear test set-ups, when one of the two bonded sides starts failing, the system loses the original symmetry and the alignment between the axis of the tensile machine and the bond surfaces; therefore, additional peeling stresses occur on one side of the specimen with the consequent reduction of the transmissible force on that side and the sudden failure of the FRP reinforcement. This phenomenon makes uncertain the definition of the effective tensile load applied to each bonded side, and very difficult the experimental monitoring of the nonlinear bond behaviour. In general, the onset of a not symmetric behaviour in a double-shear scheme may start even at the beginning of the test, due to imperfections and asymmetries in the application of the tensile loads to the FRP reinforcements, with a significant reduction of the bond capacity, especially for short bonded lengths (Yao et al. 2005). For increasing bonded lengths, the effect of misalignments or imperfections tends to be smaller.

In the single push shear test only one concrete block is tested and usually two schemes are realized in the laboratories. In the first one the concrete block is placed in a stiff steel frame with an upper plate compressing the specimen, while the end of the FRP reinforcement is clamped in the grips of a tensile machine (see Fig. 3.18a, b, McSweeney and Lopez 2005; Ceroni et al. 2008). In the second one, the specimen is placed on an horizontal plane (see Fig. 3.18c, d, Yao et al. 2005; Mazzotti et al. 2005; Matana et al. 2005; Ceroni et al. 2014), the concrete block is restrained at the free end by a mechanical anchorage and contrasted at the loaded end by a steel block. These two set-ups can give some differences in terms of debonding loads due to the different restraint conditions of the concrete blocks. In Mazzotti et al. (2013), indeed, a difference of about 10–15 % for the debonding loads was observed in the two set-ups for bond tests carried out on equal specimens. A possible explanation can be found considering that in the horizontal set-up the concrete face opposite to the FRP bonded one is prevented from transverse displacement (Fig. 3.19a); on the contrary, the same surface in the vertical set-up is completely free from restraints (Fig. 3.19b). For this reason, when the tensile load is applied to the FRP reinforcement a bending moment occurs due to the misalignment of the two forces (action and reaction), eventually inducing a deformation of the concrete prism generating peeling stresses in the FRP reinforcement that can reduce the bond strength. A 3D FE model confirmed the differences in terms of debonding loads experimentally observed using the two set-ups. The comparison of the experimental strains measured in the two schemes showed that, as the load increases, the longitudinal strains along the direction of the fibers in the vertical set-up become generally higher than strains from the horizontal one due to the additional flexural deformation.

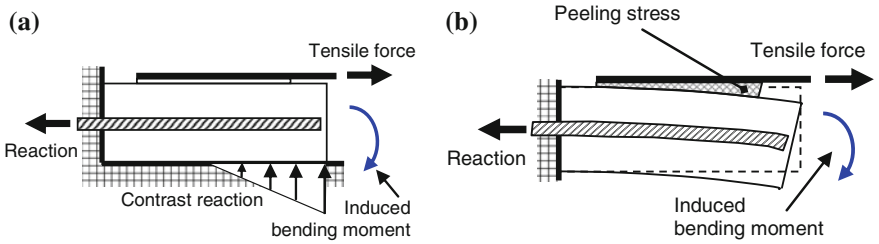

Fig. 3.19 Deformation mechanism of the concrete block in the push shear set-up: **a** horizontal scheme; **b** vertical scheme

A recent Italian round robin test has shown the reliability of the single push shear test set-up and the good repeatability of the results in terms of debonding loads (Savoia et al. 2009).

In the beam test set-up, well known for characterization of bond behaviour of steel bars in concrete elements according to the RILEM standards, the tension force is applied to the FRP reinforcement by a flexural scheme. Two blocks, placed on supports, are connected at bottom by the FRP reinforcement and above by a cylindrical hinge. Two vertical loads are generally applied (Cruz and Barros 2002; De Lorenzis et al. 2001; Ceroni et al. 2003). In some cases beam tests have been performed on a single concrete prism having a steel plate or a notch in the middlespan aimed to promote the formation of a crack in that position (Guo et al. 2005; Dai et al. 2003). However, the loading pattern of the beam test can cause a shear failure in the blocks for lower length/height ratios (Ceroni and Pecce 2006) that avoids attaining the actual bond strength.

Comparison of Experimental Results of Different Set-Ups

In order to compare experimental results coming from different set-ups, they have been compared with the theoretical expression given by Chen and Teng (2001) for the maximum debonding load:

$$N_{f,\max} = \alpha \cdot \beta_p \cdot \beta_L \cdot b_f \cdot L_e \cdot \sqrt{f_c'}\,;\; L_e = \sqrt{\frac{E_f \cdot t_f}{\sqrt{f_c'}}};$$
$$\beta_p = \sqrt{\frac{2 - b_f/b_c}{1 + b_f/b_c}}; \tag{3.20}$$

$$\beta_L = \sin\frac{\pi L_b}{2L_e} \text{ if } L_b \le L_e, \quad \beta_L = 1 \text{ otherwise} \tag{3.21}$$

where b_f, t_f, E_f and L_b are width, thickness, Young's modulus, and bonded length of the FRP reinforcement, b_c is the width of the concrete element, f'_c is the mean cylindrical compressive strength of concrete and α is a calibration factor equal to 0.427 or 0.315 to calculate the mean value or the 5 % percentile of debonding load, respectively.

The considered experimental results have been obtained in bond tests carried out according to various set-ups:

- beam tests, named BT, (De Lorenzis et al. 2001; Cruz and Barros 2002; Guo et al. 2005; Aiello and Leone 2005; Dimande et al. 2005; Wang et al. 2005; Ceroni and Pecce 2006);
- pull shear tests, named PlST, (Brosens and van Gemert 1997; Maeda et al. 1997; Ueda et al. 1999; Wu et al. 2001; Ceroni and Pecce 2002; Aiello and Leone 2005; Boschetto et al. 2006; Yi et al. 2006);
- and push shear tests, named PsST, (Chajes et al. 1996; Takeo et al. 1997; Ueda et al. 1999; Zhao et al. 2000; Wu et al. 2001; Coronado and Lopez 2005; Lu et al. 2005; McSweeney and Lopez 2005; Pham and Al-Mahaidi 2005; Yao et al. 2005; Travassos et al. 2005; Leone et al. 2006; Savoia et al. 2009).

In the experimental database results of specimens with bonded length less than 50 mm, FRP width lower than 40 mm, and Young's modulus lower than 80,000 MPa were excluded; 448 experimental points have been collected. These limits have been fixed in order to reduce the scatter of the results, to exclude from the calibration procedure the results related to unrealistic strengthening configurations that can be strongly influenced by scale effects (too short bonded length or too low width and, thus, too low FRP-to-concrete width ratio), and to avoid the materials with elastic properties too different from those usually adopted in the experimental tests and in the practical applications. Thus, the main parameters of specimens are variable in the following ranges: concrete width, b_c = 100–500 mm, FRP width, b_f = 40–120 mm, b_f/b_c = 0.17–1, FRP thickness, t_f = 0.083-1.4 mm, number of layers, n = 1–6, Young modulus of fibers, E_f = 81380–640000 MPa, bonded length, L_b = 50–700 mm, mean compressive strength of concrete, f_{cm} = 17–62 MPa, mean tensile strength of concrete, f_{ctm} = 1.30–4.30 MPa.

In Fig. 3.20 the experimental debonding loads, distinguished according to the different set-ups (Fig. 3.20a for beam tests, Fig. 3.20b for pull tests, Fig. 3.20c for push test) are compared with the theoretical mean values given by Eq. (3.20) (i.e. the parameter α is assumed 0.427) and in Table 3.2 a summary of these comparisons is reported in terms of mean value, standard deviation, and CoV of the experimental–to-theoretical debonding load ratio, $N_{exp}/N_{f,max}$.

For the beam test (BT) the model underestimates the experimental results (the average value of $N_{exp}/N_{f,max}$ is indeed ≥1) with CoV values comparable with the push shear tests (0.21—0.27). The higher experimental loads obtained for such a

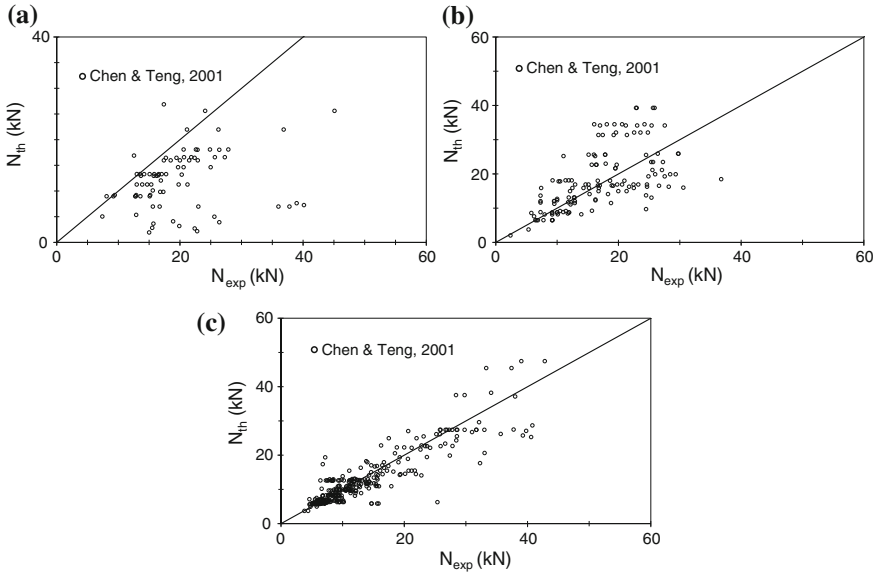

Fig. 3.20 Experimental results versus theoretical debonding load by Eq. (3.1): **a** beam test (BT); **b** pull shear test (PlST); **c** push shear test (PsST) single or double

Table 3.2 Statistical summary of experimental to theoretical debonding load ratio

	$N_{exp}/N_{f,max}$	
Beam test (61 data)	Mean	1.30
	Stand. dev	0.27
	CoV	0.21
Pull shear test (115 data)	Mean	0.98
	Stand. dev	0.36
	CoV	0.36
Push shear test (272 data)	Mean	1.01
	Stand. dev	0.23
	CoV	0.22
All results (448 data)	Mean	1.04
	Stand. dev	0.29
	CoV	0.28

set-up could be related to the length-to-height ratio of the concrete block that could not lead to a real 'debonding failure'. Indeed, the dimension of the block could activate an 'arc' resistant mechanism that allows transferring a lower tensile force to the external FRP plate compared to the 'beam' mechanism and higher stresses in the concrete strut that results in a shear failure.

For the pull shear tests (PlST) the theoretical formula overestimates the experimental results (the average value of $N_{exp}/N_{f,max}$ is indeed ≤1) and the CoV is higher

(0.36–0.42) than other set-ups; these results are probably due to the crucial influence of imperfections of specimens.

The results of the push shear tests (PsST) seem to be well replicated by the models: the average value of $N_{exp}/N_{f,max}$ is very close to 1 and the CoV values are the lowest (0.22–0.25).

If the results of all set-ups are considered, the synthesis reported in Table 3.1 shows that Eq. (3.19) furnishes an average value of $N_{exp}/N_{f,max}$ lightly ≥ 1, with a reliable value of CoV (0.28).

Intermediate Debonding

As shown above, in the last years huge research efforts have been carried out for understanding the behavior of reinforced concrete beams strengthened by externally bonded FRP. The main subject of these studies is the mechanical characterization of the FRP-to-concrete adhesive interface and particularly the investigation of the plate end debonding and intermediate debonding. Nevertheless, formulations to describe the FRP-to-concrete bond behavior are still under discussion. Various proposals have been derived from simplified mechanical models and calibrated making use of the experimental results available in the scientific literature (Teng et al. 2002). Alternatively numerical simulations allow to simulate and, thus, further investigate the debonding phenomenon. Roberts (1989) provided a simplified model for evaluating interface stresses in FRP (or even steel) strengthened beams; simplified equations for evaluating shear and normal stresses throughout the FRP-to-concrete interface have been provided by assuming linear elastic behavior of the adhesive interface. Similar relationships, even obtained under simplified hypotheses for the interface behavior, have been provided in Malek et al. (1998). The authors showed, through experimental and numerical comparisons, that such simplified formulae usually result in a close approximation of the complex stress patterns which develop throughout the FRP-to-concrete interface.

The above mentioned research papers mainly deal with interface stress distribution in the elastic range, which is an aspect of concern for serviceability conditions. Premature loss of bonding between FRP and concrete needs to be studied by considering a suitable non-linear relationship between interface stresses and strains. Holzenkaempfer (1994) proposed a bi-linear relationship between shear stresses and interface slips; based on such model Taljsten (1997a, b) determined the expressions of the ultimate bearing capacity of FRP-to-concrete joints.

In Faella et al. (2006a, b) a numerical model is implemented and validated: the study is mainly focused on debonding failure which can occur at the FRP-cut-off section (plate end debonding) or throughout the FRP-to-concrete adhesive interface (intermediate debonding). Interface slips between reinforced concrete beam and FRP laminates are considered and, consequently, a well-established non-linear shear stress-slip law is introduced. Moreover, non-linear stress-strain relationships are utilized for modeling the other structural materials and a completely non-linear

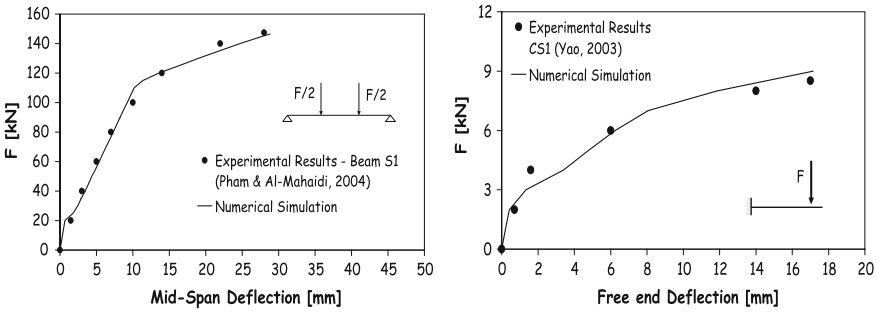

Fig. 3.21 Experimental and numerical Load-Deflection curves. (Faella et al. 2008a)

analysis procedure is obtained by means of a secant approach; such non-linear procedure allows for reproducing the whole structural behaviour up to failure which can be due to FRP tearing, concrete crushing or interface debonding. Figure 3.21 shows how the complete evolution of the displacement-vs-force curve recorded for a simply supported beams (Pham and Al Mahaidi 2004) and a cantilever beam (Yao et al. 2005) externally strengthened by FRP can be followed by the numerical procedure which provides also a good estimation of the ultimate load and displacement.

A high level of uncertainty still overshadows the mechanical understanding of intermediate debonding due to the complex interactions between several phenomena, such as cracking in concrete, steel yielding in longitudinal rebars, interface adhesion properties, the amount of reinforcement, the load condition and so on. As a result of this incomplete understanding of the mechanical reasons leading to intermediate debonding failure of FRP-strengthened RC beams, several analytical approaches have been proposed within the scientific literature and adopted by the most common design codes. Since those procedures work in rather different ways involving various parameters and adopting different relationships for defining interface properties, they generally lead to rather different predictions of the ultimate load resulting in intermediate debonding. Moreover, such procedures actually neglect or disregard the role played by several mechanical parameters in controlling the structural response of FRP-strengthened RC beams, adopting simplified expressions for deriving formulae usually calibrated on the available experimental observations.

Two different methodological paths can be followed for defining reasonably simplified design formulae based on experimental results:

– direct calibration of empirical expressions against experimental results by means of well-established mathematical procedures like least-square minimization of the overall difference between the experimental observations and the corresponding analytical values;

– validation of refined numerical models (i.e. based on finite element discretization) by means of a limited number of experimental results and extrapolation of those results by means of the above mentioned numerical procedures.

Despite of several proposals, numerical models are not yet suitable to take into account all phenomena affecting debonding. Therefore, a simplified design formula (see Chap. 2—Application 3) based on a statistically consistent procedure for determining the safety levels required for defining the so-called "characteristic" and "design" values of the maximum axial strain developed in FRP at intermediate debonding is probably more useful for design purposes.

Figure 3.22 shows a comparison between design curves obtained in Chap. 2—Application 3 and other curves according to some of the models outlined in Sect. 3. Both the model by Said and Wu (2008) and the formula adopted by ACI440-08 lead to predictions in terms of maximum axial strain in FRP at debonding which are not conservative enough to be used for design purposes. Moreover, the predictions based on the model by Teng et al. (2004) are rather close to the values obtained by the current CNR-DT 200/2004 provisions. In the case of low concrete strength (namely, for $f_c < 40$ MPa), both formulations look not conservative enough for design purposes.

On the other hand, the predictions obtained by applying the formulation in Chap. 2 by considering the $k_{IC,5\ \%}$ coefficient, a further safety factor $\gamma_{f,d} = 1.2$ addressing the quality of the application, a confidence factor $FC = 1$ as "full knowledge" is achieved about the mechanical properties of structural materials demonstrate the higher level of conservativeness achieved by this proposed formula. Finally, although the curves representing the results of the model by Teng et al. (2003) are generally even more conservative than those obtained by the model proposed in Chap. 2, it could result in too strict provisions for a cost-effective

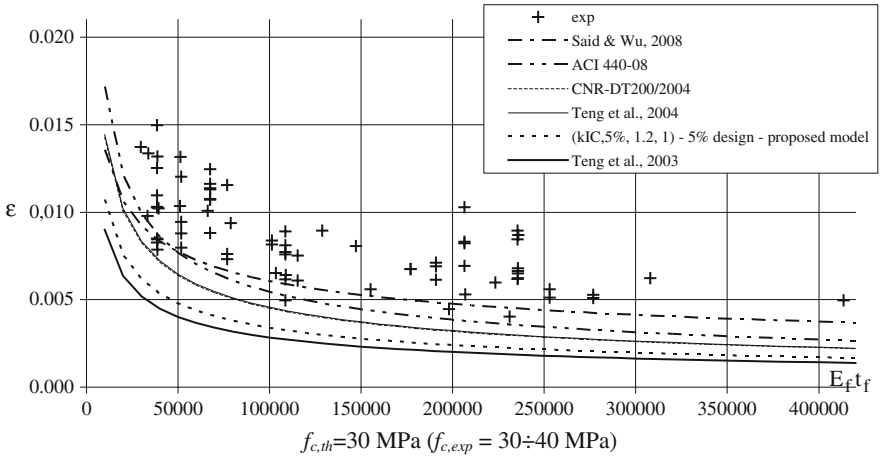

Fig. 3.22 Experimental results and code provisions

application of FRP strengthening. The two curves representing the design formula and the model by Teng et al. (2003) are rather close but the former can move upward if a unit value is also considered for $\gamma_{f,d}$, as a result of a certified application procedure allowing for higher values of the relevant mechanical properties of the adhesive-to-concrete interface.

Bond Law Identification Method

The FRP-to-concrete interface behaviour is often described by its fracture energy G_F, which is directly related to the ultimate load F_{max} observed in pull-out tests. Nevertheless, assessing the G_F value is not sufficient for reproducing the overall behaviour of the FRP-to-concrete interface for modeling problems such as, for instance, intermediate debonding in RC beams externally strengthened by FRP reinforcement (Faella et al. 2008a). Thus, an accurate local bond–slip model is of fundamental importance in modeling FRP-strengthened RC elements.

As showed in the previous sections, the pull test delivers the ultimate load of the FRP-to-concrete interface, but can also provide useful information on the local bond–slip behaviour of the interface if axial strains of the FRP reinforcement are measured with closely spaced strain gauges. Indeed, the shear-stress-relative-slip relationship, describing the FRP-to-concrete interface law, can be identified starting from the values of the strains recorded during the tests at different load levels.

Commonly, the shear stress of a particular location along the FRP-to-concrete interface can be found using a difference formula, whereas the corresponding slip can be found by a numerical integration of the measured axial strains of the FRP.

In particular the interface shear stresses $\tau_i(z)$ can be obtained by the variation of axial stresses, and thus strains, throughout the FRP by the following relationship between two strain gauges at distance Δz_i:

$$\tau_i = \frac{\varepsilon_{i+1} - \varepsilon_i}{\Delta z_i} \cdot E_f \cdot t_f \tag{3.22}$$

where E_f and t_f are FRP Young's modulus and thickness, respectively. Typical shear stress profiles assessed for sheets and plates, respectively, are reported in Fig. 3.21a, b. Note that, at the loaded end of the reinforcement, shear stresses assessed for loads close to the debonding of the reinforcement are lower than those assessed for lower loads. This indicates that in this zone of the reinforcement the shear stress-slip law is in the softening stage typical of a post-elastic behaviour.

On the other hand, assuming for the sake of simplicity that concrete strain is negligible with respect to FRP counterpart, the slip values corresponding to the shear stress values obtained by Eq. (3.21) can be calculated by integrating the axial strains measured during the test by the following relationship:

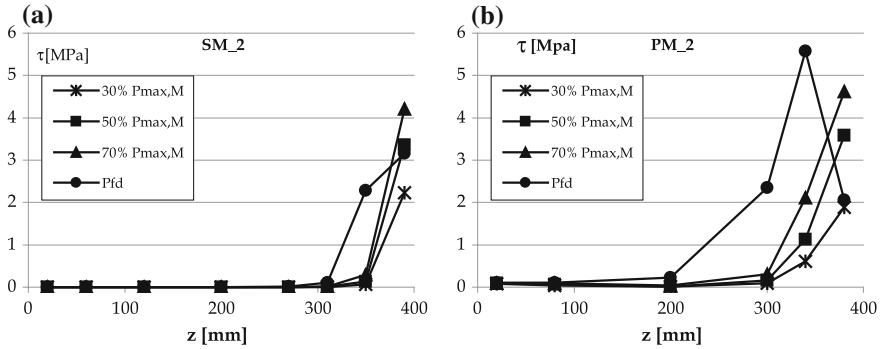

Fig. 3.23 Shear stresses assessed on sheet **a** and plate **b** reinforced specimens

$$s_{i,i+1} = \sum_{k=0}^{i} \frac{(\varepsilon_{k+1} + \varepsilon_k)}{2} \cdot (x_{k+1} - x_k) \tag{3.23}$$

Therefore, the bond law at the FRP-to-concrete interface can be obtained by calculating the shear stresses using Eq. (3.22) (considering the strains recorded by the first two gauges—e.g. at 400 and 380 mm in Fig. 3.23) and the corresponding slips using Eq. (3.23) (considering all the strain gauges applied on the FRP reinforcement). In this way the experimental interface law is obtained directly with respect to values of shear stresses and relative slips based on experimental strains (see Fig. 3.24).

Moreover, the couples of values $(\overline{s_j}, \overline{\tau_j})$ can be "directly" used to calibrate the τ-s relationship through a numerical regression, such as the least square method. This method (called DirIM in Faella et al. 2009) is very simple, but it does not often produce accurate local bond–slip curves. In particular the shear stress deduced from

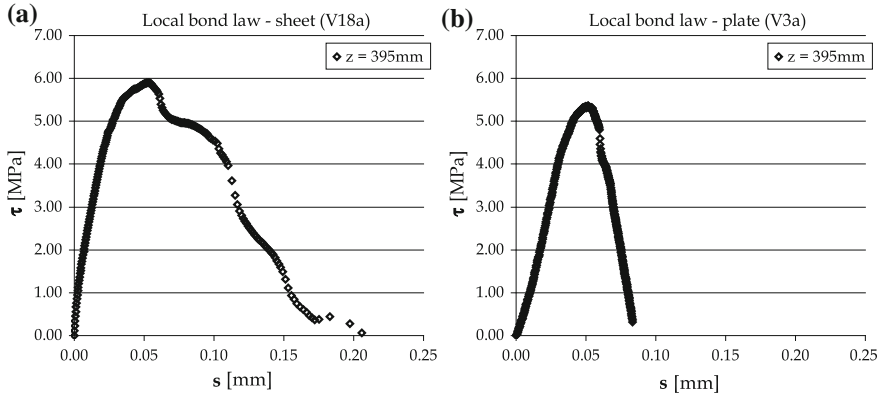

Fig. 3.24 Experimental bond law at the FRP-to-concrete interface: sheet **a** and plate **b**

axial strains can be not reliable due to sensitivity to the distance between strain gauges in the averaging procedure needed for estimating shear stresses. Consequently the method can noticeably underestimate the values of fracture energy and provide bond–slip curves, attained from different tests, substantially different.

In this regard, Ferracuti et al. (2007) presented a procedure to calibrate non-linear FRP-to-concrete interface laws from experimental results of bond tests: strains along the composite are used to obtain shear stress–slip data, whereas the maximum transmissible force is used to prescribe the value of fracture energy, G_F, of interface law. Hence, the non-linear interface law is obtained by a DirIM, taking into account a restraint on G_F in the calibrating procedure. The interface law is then used to simulate the tests and a good agreement between numerical and experimental results are showed. Nevertheless, the distribution of shear stresses cannot be directly compared with data provided by the pull out tests, because both interface shear stresses and local displacements cannot be directly measured during the usual pull-out tests.

In Lu et al. (2005), some existing bond–slip models was presented and assessed using the results of some pull tests on simple FRP-to-concrete bonded joints, leading to the conclusion that a more accurate model, unaffected by such uncertainties, is required. For this reasons three new bond–slip models of different levels of sophistication were proposed, highlighting a novel aspect in calibrating the models on the predictions of a meso-scale finite element model. Through comparisons with the test database, all three bond–slip models are shown to provide accurate predictions of both ultimate load and strain distribution in the FRP reinfocement. In particular it was showed that, while a more precise bond-slip model should consist of a curved ascending branch and a curved descending branch (see also Savoia et al. 2003 and Ferracuti et al. 2007), also other shapes such as a bilinear model can be used as a good approximation.

Among the three models proposed in Lu et al. (2005), the last is just represented by a bilinear law, identified by the following relationships for determining the three parameters τ_{max}, s_e and s_u:

$$\tau_{\max} = 1.5\beta_w f_t, \tag{3.24}$$

$$s_e = 0.015\beta_w f_t, \tag{3.25}$$

$$s_u = \frac{2.G_F}{\tau_{\max}} = \frac{2 \cdot 0.308 \cdot \beta_w^2 \cdot \sqrt{f_t}}{1.5 \cdot \beta_w \cdot f_t} = 0.41 \cdot \beta_w \cdot \sqrt{f_t} \tag{3.26}$$

where f_t is the tensile strength of the concrete and β_w is a well-known geometrical factor (as function of the ratio between the width of the FRP and the concrete member which the FRP is applied on). Slightly dissimilar expressions were suggested in literature for this factor (Lu et al. 2005; Teng et al. 2002; CNR-DT 200 2004; fib Bulletin 14 2001), but the difference among the expressions is however very small and all the mentioned equations are suitable for practical applications. Note that, for simplicity and uniformity, some relationships were formally rewritten.

It is worth observing that the relationships (23–25) were assessed by using the experimental results of bond tests performed on sheets (i.e. wet-lay-up system characterized by thickness ranging between 0.133 and 0.5 mm for one or three layers). Very few experimental data was related to tests performed on plates (i.e. preformed system characterized by thickness ranging between 1 and 2 mm) whereas the reinforcement thickness particularly affects debonding behaviour: indeed, the greater the thickness, the higher the increase in the normal and shear stresses at FRP to concrete interface and consequently the probability of premature debonding occurrence (Oehlers and Moran 1990; Tounsi et al. 2009). Even if the numerical analysis may take into account this parameter, the comparison performed with the experimental data appears clearly lacking from this point of view.

By contrast, recently (Bilotta et al. 2011b), in order to assess a design formulation to predict the plate end debonding load in RC elements strengthened with Externally Bonded Reinforcement (EBR) made of FRP materials by means of a statistical analysis, the experimental debonding loads of several bond tests available in the literature have been collected. Cured in situ (sheets) and preformed (plates) FRP systems have been distinguished to better exploit the performance of the former ones, as concerns the plate end debonding failure. Lu et al. (2005) suggested an expression for assessing the interface relationship and consequently the fracture energy value that takes into account the strength of the concrete, but completely neglects the influence of the reinforcement properties, in particular the FRP thickness. This assumption, regardless of the value of β_w, lead to same values of maximum shear stress for plates and sheets applied on the same concrete.

Thus, based on such results and the outcomes of Yao et al. (2005); Ferracuti et al. (2007); Faella et al. (2009) and Bilotta et al. (2011b), the IndIM procedure and the bilinear shape for the bond law were extensively used in Bilotta et al. (2012) with the final aim of calibrating bilinear interfaces laws, as stable as possible, and assessing their reliability for sheets and plates, separately.

Since relevant measures of shear stresses and corresponding relative strains cannot be directly obtained by pull-out tests, an alternative procedure using the experimental measures in terms of axial strain values $\varepsilon_{f,j,i}$ recorded at distance z_j under the force F_i was adopted for "indirectly" calibrating the τ-s interface relationship. The simple but effective bilinear model is taken because closed-form solutions are available for such shape of the interface law, as extensively shown in Faella et al. (2003). This model is defined by well-known relationships in which three parameters identify the bond law: the maximum shear stress, τ_{max}, the

corresponding slip, s_e, and the ultimate slip, s_u, beyond which the interface shear stress can be considered null.

Therefore, for each set, q, of parameters τ_{max}, s_e and s_u a given interface law is defined, and the corresponding theoretical value $\varepsilon_{fth,j,i}$ of the axial strain developed in the FRP plate at a distance z_j under the force F_i can be evaluated. Even if numerical procedures, such as finite differences, can generally be utilized, the choice of a bilinear bond law allowed for using the closed-form solutions (Faella et al. 2003) taking also into account, if necessary, the influence of the parameter bond length, L, in the solution of the problem.

The identifying procedure was applied on a wide collection of experimental results attained by pull tests during which not only the load but also the corresponding axial strains of the FRP reinforcement were measured. Both the consistency of IndIM method and the robustness of the assumption on the bond law shape was showed by a comparison, in terms of axial strains throughout the bonded length, between theoretical predictions and the corresponding measured values. Even if the uncertainness in accurately identifying the parameter s_e indicated that the bond behaviour in the elastic stage was not perfectly approximated by a linear branch, the result obtained by assuming a bilinear law were satisfying.

Finally, several bond law relationships, identified by three parameter (i.e. the maximum shear stress, τ_{max}, the corresponding elastic slip, s_e, and the ultimate slip, s_u), have been compared. The elastic and ultimate slips, s_e and s_u respectively, are on average the same for sheets and plates, although the dispersions of the values obtained by the identifying method are somewhat high. Conversely the values of maximum shear stress, τ_{max}, obtained for sheets bond laws are always higher than those obtained for plates interface relationships, of about 30 % in average. Clearly the same differences are attained in terms of fracture energy. Such results are in agreement with the theoretical strength models available in the literature for predicting debonding of sheets and plates separately, confirming the advisability of assessing a bond law for the plates different from that for the sheets.

Existing Models and Code Formulations

Externally bonded FRP sheets are currently used to repair and strengthen existing reinforced concrete (RC) structures for shear and flexural applications. Proper design against various debonding failure modes is the key issue of this technique (Taljsten 1997a, 1997b; Bizindavyi and Neale 1999; Chen and Teng 2001; Nakaba et al. 2001; Lu et al. 2005; Ferracuti et al. 2007; Pellegrino et al. 2008). Typical failure modes include cover separation, plate end interfacial debonding, intermediate flexural crack-induced interfacial debonding, and critical diagonal crack-induced interfacial debonding, as described in the Italian guidelines CNR-DT 200 2004. Furthermore, some authors (e.g. Yuan et al. 2004) pointed out that, although there exist many experimental setups to evaluate the FRP-concrete bond strength, a standard test procedure does not exist yet. The most diffused

experimental setups are represented by the so-called direct shear tests, single and double, and by the bending/beam test. In bending tests the FRP composite is bonded to the bottom of a beam subjected to flexure. Bending tests are sometimes carried out on small scale specimens where a notch or a hinge is provided in order to initiate debonding at a specific cross-section. The combination of results related to both small- and full-scale specimens is arguable due to different mechanisms and resisting contributions developing in small- and full-scale beams. For this reason, in this work the experimental tests of small-scale notched beams were discarded and only the results of full-scale strengthened RC beams subjected to bending tests were included in the database.

A wide assessment of some diffused analytical models available in literature was performed. Since it has been shown that these different kinds of approaches can lead to different results for the same amount and preparation of FRP and concrete support (Yuan et al. 2004), various test setups (single shear test, double shear test and bending test) and FRP composites preparation (pre-impregnated laminates and post-impregnated sheets) have been considered in the assessment. A comparison between experimental and analytical values of the bond strength and of the effective bond length is presented and discussed. The analytical models considered in this chapter are some of the most diffused formulations and include those adopted by the fib Bulletin 14 (2001), CNR-DT 200 (2013) and ACI 440.2R-08 (2008).

Theoretical Models

A number of analytical bond formulation have been proposed in literature by several authors, have been considered in this work and are briefly recalled for the sake of clarity.

van Gemert (1980):

$$N_f = 0.5 \cdot b_f \cdot l_b \cdot f_{ctm} \tag{3.27}$$

Tanaka (1996):

$$N_f = (6.13 - \ln l_b) \cdot b_f \cdot l_b \tag{3.28}$$

Hiroyuki and Wu 1997:

$$N_f = 5.88 \cdot l_b^{-0.669} \cdot b_f \cdot l_b \tag{3.29}$$

Maeda et al. 1997:

$$N_f = 110.2 \cdot 10^{-6} \cdot E_f \cdot t_f \cdot b_f \cdot l_e \tag{3.30}$$

Neubauer and Rostàsy 1997:

$$N_f = 0.64 \cdot k_p \cdot b_f \cdot \sqrt{f_{ctm} \cdot E_f \cdot t_f} \tag{3.31}$$

when $l_b \geq l_e$.

$$N_f = 0.64 \cdot k_p \cdot b_f \cdot \sqrt{f_{ctm} \cdot E_f \cdot t_f} \cdot \frac{l_b}{l_e} \cdot \left(2 - \frac{l_b}{l_e}\right) \tag{3.32}$$

when $l_b < l_e$.

Khalifa et al. (1998):

$$N_f = 110.2 \cdot 10^{-6} \cdot \left(\frac{f_{ck}}{42}\right)^{2/3} E_f \cdot t_f \cdot b_f \cdot l_e \tag{3.33}$$

Adhikary and Mutsuyoshi (2001):

$$N_f = b_f \cdot l_b \cdot \left(0.25 \cdot f_{ck}^{2/3}\right) \tag{3.34}$$

Chen and Teng 2001:

$$N_f = 0.315 \cdot \beta_p \cdot \beta_L \cdot \sqrt{f_{ck}} \cdot b_f \cdot l_e \tag{3.35}$$

De Lorenzis et al. 2001:

$$N_f = b_f \cdot \sqrt{2 \cdot E_f \cdot t_f \cdot G_f} \tag{3.36}$$

Yang et al. (2001) (in Lu et al. 2005):

$$N_f = \left(0.5 + 0.08 \cdot \sqrt{\frac{E_f \cdot t_f}{1000}}\right) \cdot b_f \cdot l_e \cdot 0.5 \cdot f_{ctm} \tag{3.37}$$

Dai et al. (2005a, b):

$$N_f = \left(b_f + 7.4\right) \cdot \sqrt{2 \cdot E_f \cdot t_f \cdot G_f} \tag{3.38}$$

Lu et al. (2005):

$$N_f = \beta_l \cdot b_f \cdot \sqrt{2 \cdot E_f \cdot t_f \cdot G_f} \tag{3.39}$$

Camli and Binici 2007:

$$N_f = \sqrt{\tau_f \cdot \delta_f} \cdot \sqrt{E_f \cdot t_f} \cdot b_f \cdot \tanh\left(\frac{\theta \cdot l_b}{l_e}\right) \tag{3.40}$$

Izumo (2003) (included and cited in the JCI 2003 Recommendations):

$$N_f = \left(3.8 \cdot f_{ck}^{2\beta} + 15.2\right) \cdot l_b \cdot b_f \cdot E_f \cdot t_f \cdot 10^{-3} \tag{3.41}$$

Iso (2003) (included and cited in the JCI 2003 Recommendations):

$$N_f = b_f \cdot l_e \cdot 0.93 \cdot f_{ck}^{0.44} \tag{3.42}$$

Sato (2003) (included and cited in the JCI 2003 Recommendations):

$$N_f = \left(b_f + 7.4\right) \cdot l_e \cdot 2.68 \cdot f_{ck}^{0.2} \cdot E_f \cdot t_f \cdot 10^{-5} \tag{3.43}$$

The analytical models just reported were applied without considering safe and partial factors to allow the comparison with the experimental data collected within the database. The details about the notation can be found in the cited papers.

Code Formulations

fib Bulletin 14 (2001)
According to the *fib* Bulletin 14 (2001) the maximum force which can be anchored by the FRP is expressed by:

$$N_{fa,\max} = \alpha\, c_1\, k_c\, k_b\, b\, \sqrt{E_f\, t_f\, f_{ctm}} \tag{3.44}$$

where:

$$k_b = 1.06\sqrt{\frac{2 - b_f/b}{1 + b_f/400}} \geq 1 \tag{3.45}$$

$$N_{fa} = N_{fa,\max}\frac{l_b}{l_{\max}}\left(2 - \frac{l_b}{l_{\max}}\right) \quad for\ l_b < l_{b,\max} \tag{3.46}$$

The effective bond length is expressed by:

$$l_{b,\max} = \sqrt{\frac{E_f\ t_f}{c_2\ f_{ctm}}} \tag{3.47}$$

CNR-DT 200 (2004)

The Italian document CNR-DT 200 (2004) proposes a formulation similar to that of the *fib* Bulletin 14 (2001); it quantifies the maximum stress in the FRP reinforcement as a function of the fracture energy of the FRP-concrete interface:

$$f_{fdd} = \frac{k_{cr}}{\gamma_{f,d}\ \sqrt{\gamma_c}} \sqrt{\frac{2\ E_f\ \Gamma_{Fk}}{t_f}} \tag{3.48}$$

$$f_{fdd,rid} = f_{fdd}\ \frac{l_b}{l_e}\left(2 - \frac{l_b}{l_e}\right) \quad for\ l_b < l_e \tag{3.49}$$

The maximum force which can be anchored by the FRP is finally calculated multiplying the area of the composite and the stress f_{fdd}.

The factor k_{cr} distinguishes between different kinds of delamination (k_{cr} = 1 for the end delamination, k_{cr} = 3 for the intermediate delamination due to flexural cracking).

The fracture energy of the FRP-concrete interface is expressed by:

$$\Gamma_{Fk} = 0.03\ k_b\ \sqrt{f_{ck}\ f_{ctm}} \tag{3.50}$$

where:

$$k_b = 1.06\sqrt{\frac{2 - b_f/b}{1 + b_f/400}} \geq 1 \tag{3.51}$$

The effective bond length is expressed by:

$$l_e = \sqrt{\frac{E_f\ t_f}{2\ f_{ctm}}} \tag{3.52}$$

The meaning of the symbols is detailed in the *fib* Bulletin 14 (2001), ACI 440.2R-08 (2008), and CNR-DT 200 (2004).

A new version of the Italian guidelines, CNR-DT 200 R1/2013 has been recently published. It provides new equations that can improve the model accuracy. Among the others, a new equation for computing the fracture energy, which has a different values depending on the material used, the effective bond length, and the FRP-concrete strength is provided. The maximum stress f_{fdd} that can be carried by the composite preventing the end plate debonding failure is calculated as:

$$f_{fdd} = \frac{k_{cr}}{\gamma_{f,d}} \sqrt{\frac{2\, E_f\, \Gamma_{Fk}}{t_f}} \tag{3.53}$$

$$f_{fdd,rid} = f_{fdd} \frac{l_b}{l_e} \left(2 - \frac{l_b}{l_e}\right) \quad for\ l_b < l_e \tag{3.54}$$

The fracture energy Γ_{Fd} is computed as:

$$\Gamma_{Fd} = \frac{k_b \cdot k_G}{FC} \cdot \sqrt{f_{cm} \cdot f_{ctm}} \tag{3.55}$$

$$k_b = \sqrt{\frac{2 - b_f/b}{1 + b_f/b}} \geq 1 \tag{3.56}$$

where $k_G = 0.023$ in case of pre-impregnated laminate, and $k_G = 0.037$ in case of post-impregnated sheet. FC is an additional safety factor. In order to avoid the intermediate crack-induced debonding failure the maximum FRP stress must be less or equal to $f_{fdd,2}$:

$$f_{fdd,2} = \frac{k_q}{\gamma_{f,d}} \sqrt{\frac{E_f}{t_f} \cdot \frac{2 \cdot k_b \cdot k_{G,2}}{FC} \cdot \sqrt{f_{cm} \cdot f_{ctm}}} \tag{3.57}$$

where $k_{G,2}$ is an empirical coefficient equal to 0.10, and $k_q = 1.25$ in case of distributed load, and $k_q = 1.0$ in all other cases. The CNR-DT 200 R1/2013 computes the effective bond length, named optimum bond length, as:

$$l_e = \min\left\{\frac{1}{\gamma_{Rd} \cdot f_{bd}}\sqrt{\frac{\pi^2 \cdot E_f \cdot t_f \cdot \Gamma_{Fd}}{2}},\ 200\right\} \tag{3.58}$$

$$f_{bd} = \frac{2 \cdot \Gamma_{Fd}}{s_u} \tag{3.59}$$

where $s_u = 0.25$ is the ultimate slip between the FRP and the concrete support, and $\gamma_{Rd} = 1.25$ is a modification factor.

ACI 440-2R-08 (2008)

According to ACI 440.2R-08 (2008) the maximum bond strength is calculated multiplying the maximum strain in the FRP reinforcement at the ultimate limit state by the fibre elasticity modulus, assuming perfectly elastic behaviour. The effective strain in FRP reinforcement is limited to the strain level at which debonding may occur, ε_{fd}, as defined in Eq. (3.60). The ultimate strength of the structural member is then found considering the mode of failure for an assumed neutral axis depth, as computed in Eq. (3.61).

$$\varepsilon_{fd} = 0.41\sqrt{\frac{f'_c}{nE_f t_f}} \leq 0.9\varepsilon_{fu} \tag{3.60}$$

$$\varepsilon_{fe} = \varepsilon_{cu}\left(\frac{d_f - x}{x}\right) \leq \varepsilon_{fd} \tag{3.61}$$

$$f_{fe} = E_f \varepsilon_{fe} \tag{3.62}$$

where ε_{cu} is the maximum compressive strain in the concrete, taken as 0.003; d_f and x are the depth of the FRP and the neutral axis, respectively. The maximum force which can be anchored by the FRP is finally calculated multiplying the area of the composite and the stress f_{fe}.

In case of shear or pure axial strengthening the maximum bond strength is calculated multiplying the maximum strain in the FRP reinforcement at the ultimate limit state, according to Eq. (3.63) (in case of U-Wraps or bonded face plies), by the fibre elasticity modulus, assuming perfectly elastic behaviour as in the flexural case (Eq. 3.64). k_v is an empirical coefficient limiting the ultimate strain in the reinforcement:

$$\varepsilon_{fe} = k_v\ \varepsilon_{fu} \leq 0.004 \tag{3.63}$$

$$k_v = \frac{k_1\ k_2\ l_e}{11{,}900\ \varepsilon_{fu}} \leq 0.75 \tag{3.64}$$

where k_1 and k_2 are taken equals to 1.0 (case of pure axial tension). The active bond length, i.e. the length over which the majority of the bond stress is maintained, is expressed by:

$$l_e = \frac{23{,}300}{(n_f t_f E_f)^{0.58}} \tag{3.65}$$

Assessment of Code Formulations Pellegrino

The experimental database used for the assessment of the considered FRP-to-concrete bond analytical models contains 410 specimens, 229 tested with single shear test setup (Bizindavyi and Neale 1999; Chen and Teng 2001; Yao et al. 2005; Lu et al. 2005; Toutanji et al. 2007; Ceroni and Pecce 2010), including both laminates (45 specimens) and sheets (184 specimens); 60 sheet specimens tested by double shear test setup (Chen and Teng 2001; Lu et al. 2005; Pellegrino et al. 2008); 121 specimens tested with bending test setup (Ahmed et al. 2001; Fanning and Kelly 2001; Rahimi and Hutchinson 2001; Smith and Teng 2002; Teng and Yao 2007, Pellegrino et al. 2008), including both laminates (74 specimens) and sheets (47 specimens).

In Fig. 3.25 a comparison between experimental and analytical values, obtained by fib Bulletin 14 (2001), CNR-DT 200 (2004), ACI 440.2R-08 (2008), and CNR-DT 200 R1/2013 for different experimental setups (single shear, double shear, bending test), and different composite materials (laminates and sheets) is shown.

The assessment was carried out by means of a statistical procedure. The performance of the analytical model for evaluating the maximum bond strength of the FRP-concrete interface was obtained comparing the experimental values with the corresponding analytical predictions. As usual, experimental versus theoretical bond diagrams have been built. The values above the line $P_{exp}/P_{th} = 1$ (where P is the force pulling the composite) are safe, whereas values below are unsafe. The accuracy of the various models was assessed through the use of a coefficient of variation (CoV), which measures the distance between the ratio P_{exp}/P_{th} and the optimum ideal value $P_{exp}/P_{th} = 1$.

Using the database herein described, a comparison between experimental and theoretical values for different experimental setups, namely single shear test, double shear test and bending test, was performed. A comparison between experimental and theoretical values for different composite materials, namely laminates and sheets, was made as well.

Table 3.3 summarizes the results of the statistical analysis in terms of maximum force carried by the FRP-concrete bond surface. The value of the CoV together with the indication of the corresponding mean value of the ratio between the experimental and theoretical value (Avg), are provided.

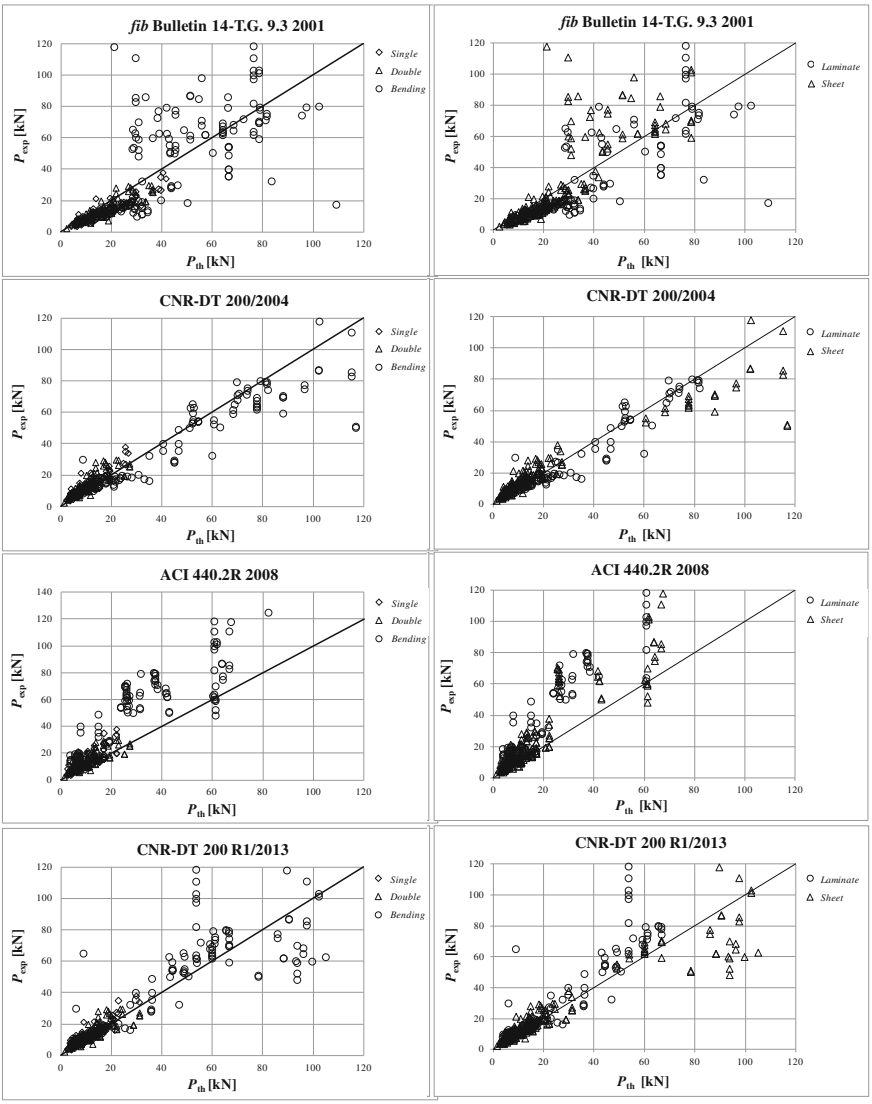

Fig. 3.25 Comparison between experimental and analytical values for different experimental setups (single shear, double shear, bending test), and different composite materials (laminates and sheets)

The analytical formulations for the effective bond length were compared to the experimental measurements for different material preparations (pre-impregnated laminates and post-impregnated sheets). Since there are few works in which the effective bond length was experimentally measured due to the practical difficulty of the procedure, the database was comprised of 48 specimens taken from

Bizindavyi and Neale (1999), Pellegrino et al. (2008), Subramaniam et al. (2007, 2011), Carloni et al. (2012), Carloni and Subramaniam (2013), and Nguyen et al. (2001).

Table 3.4 summarizes the results of the statistical analysis for the effective bond length. The value of the CoV together with the indication of the corresponding average value of the ratio between the experimental and theoretical value (Avg), the standard deviation (StD), and the percentage of the overestimated length value (OverE), are provided.

Critical Issues of Models and Experimental Procedures

Considering the analysis of the laminates and sheets together (*Sheet* + *Laminate* in Table 3.3), the results show that the analytical formulations for the evaluation of the FRP-concrete bond strength are sometimes non conservative. The better result in terms of coefficient of variation (CoV) was obtained with the model proposed by Camli and Binici (2006) although it provides more scattered results in case of bending tests rather than single- and double-lap direct-shear tests. The ACI 440.2R-08 (2008) provides more conservative prediction in terms of maximum FRP-concrete bond strength (Figs. 3.25 and 3.26) with respect to the other codes, thou its accuracy is rather poor.

The statistical analysis of the various set-ups showed that some models provide better results using the single-lap direct-shear test whereas others using the double-lap direct-shear test, probably depending on which set-up the authors used to formulate the model. In general, except in case of the Italian CNR-DT 200 (2004), the analytical predictions seem to be particularly inaccurate in case of full-scale bending test. The new version of the Italian guidelines, CNR-DT 200 R1/2013, provides better results with respect to the previous version both in case of single- (CoV = 0.44), and double-lap (CoV = 0.42) direct-shear test. When applied to full-scale bending tests, the CNR-DT 200 R1/2013 seems to be particularly inaccurate (CoV = 0.76), especially if compared with the result obtained with the previous version (CoV = 0.39). The same issue arises when the analytical model of the CNR-DT 200 R1/2013 is applied to the tests carried out using pre-impregnated laminate (CoV = 0.91, 2.1 times higher with respect to the previous version). This inaccuracy affects the overall results of the model (CoV = 0.55). It should be noted that 75 % of the full-scale bending test results included within the database are carried out using pre-impregnated laminate. For this reason it is not possible to evaluate whether the model proposed by the CNR-DT 200 R1/2013 is inaccurate when applied to full-scale bending tests or to pre-impregnated laminate.

Observing the effective bond length versus FRP stiffness ($E_f t_f$) diagram (Fig. 3.26h) it can be seen that the predictions are good for low values of the FRP stiffness, whereas become worse for higher values. The ACI 440.2R-08 (2008) model showed an opposite trend with respect to the other main formulations. The best result for effective bond length, in terms of CoV, was obtained by the new

Table 3.3 Main results of the statistical procedure on the maximum force carried by the FRP-concrete bond interface

Analytical model	Single		Double		Bending		Sheet		Laminate		Sheet + Laminate	
	Avg	CoV	Avg	CoV	Avg	CoV	Avg	CoV	Avg	CoV	Avg	CoV
Van Gemert (1980)	1.51	0.84	0.94	0.54	0.84	2.98	1.18	0.66	1.06	1.18	1.08	0.76
Tanaka (1996)	1.75	1.20	1.40	0.70	–	–	1.90	1.00	2.19	2.94	1.77	1.21
Hiroyuki and Wu (1997)	1.91	1.15	1.82	1.25	1.95	1.42	1.90	1.38	2.19	1.48	1.91	1.38
Maeda et al. (1997)	0.97	0.24	1.05	0.32	1.39	0.94	1.12	0.59	1.08	0.41	1.11	0.56
Neubauer and Rostásy (1997)	0.87	1.38	0.99	0.22	1.37	0.94	1.05	0.54	0.95	0.50	1.04	0.54
Khalifa et al. (1998)	1.24	0.41	1.05	0.38	1.30	0.90	1.30	0.64	1.03	0.40	1.23	0.59
fib Bulletin 14-T.G. 9.3 (2001)	0.84	0.23	0.85	0.26	1.15	0.74	0.95	0.46	0.87	0.39	0.93	0.45
Adhikary and Mutsuyoshi (2001)	0.90	0.41	0.55	0.55	0.20	0.81	0.70	0.48	0.63	0.80	0.64	0.58
Chen and Teng (2001)	1.47	1.38	1.66	0.75	2.31	1.95	1.76	1.18	1.67	1.05	1.75	1.17
De Lorenzis et al. (2001)	0.67	0.36	0.72	0.34	0.92	0.60	0.77	0.45	0.70	0.40	0.75	0.44
Izumo (2003)	0.85	0.39	0.69	0.62	0.10	0.97	0.72	0.53	0.08	1.22	0.61	0.62
Iso (2003)	1.06	0.26	0.96	0.31	1.11	0.78	1.11	0.50	0.90	0.38	1.06	0.48
Sato (2003)	0.73	0.36	0.85	0.53	0.53	0.79	0.77	0.47	0.46	0.70	0.69	0.54
Yang et al. (2003)	1.14	0.30	1.04	0.35	1.39	0.95	1.24	0.61	1.11	0.41	1.20	0.58
CNR-DT 200 (2004)	1.42	0.52	1.34	0.52	0.86	0.39	1.30	0.51	1.14	0.43	1.23	0.48
Dai et al. (2005a, b)	0.61	0.41	0.67	0.38	0.90	0.59	0.72	0.47	0.65	0.44	0.70	0.46
Lu et al. (2005)	1.00	0.18	1.17	0.32	1.62	1.18	1.22	0.68	1.14	0.57	1.21	0.67
Camli and Binici (2006)	1.01	0.31	0.84	0.37	0.62	0.55	0.93	0.35	0.80	0.51	0.87	0.40
ACI 440.2R (2008)	1.45	0.59	1.78	0.94	2.12	1.46	1.52	0.72	2.14	1.41	1.66	0.92
CNR-DT 200 R1/2013	1.30	0.44	1.22	0.42	1.14	0.76	1.19	0.37	1.41	0.91	1.24	0.55

Table 3.4 Results of the statistical analysis procedure for the FRP effective bond length carried out without distinguish between laminate and sheet composites

	OverE (%)	StD	Avg	CoV
CNR-DT 200/04	35	0.23	0.97	0.22
fib/01				
Neubauer and Rostásy (1997)				
Lu et al. (2005)	100	0.43	1.78	0.88
Chen and Teng (2001)	35	0.24	0.96	0.24
Camli and Binici (2006)				
Iso (2003)	77	0.36	1.27	0.44
Sato (2003)	0	0.20	0.63	0.41
Maeda et al. (1997)	97	4.17	5.37	5.99
Khalifa et al. (1998)				
ACI 440.2R (2008)	97	4.52	5.82	6.56

version of the Italian guidelines, CNR-DT 200 R1/2013, which improves the previous model also adopted by the fib Bulletin 14 (2001) and Neubauer and Rostasy (1997).

The results obtained show a clear influence of the test set-up on the accuracy of the analytical models. This observation is of particular importance because it highlights the needs of a standard shared test set-up. Furthermore, the poor accuracy of the analytical models when applied to full-scale RC beams show the need of further investigation on FRP strengthened RC beams.

Fib Bulletin 14 (New Formulation)

The indications provided by the most recent formulation of the fib Bulletin 14, which are still under discussion and, thus, were not considered for the previous assessment, are shown below for the sake of completeness. In the new draft of fib Bulletin 14, three types of deboding failure modes, needing specific verifications, are considered:

1. Debonding at the end anchorage zone;
2. Debonding at the end anchorage zone for Concrete Cover Delamination and Critical Diagonal Crack debonding;
3. Debonding at intermediate cracks due to shear stresses (IC Debonding);

Debonding due to unevenness of the concrete surface is also cited, but clearly no calculation is furnished, but only attention in the surface treatment. About the "*Debonding at the end anchorage zone*", under the hypothesis that in EBR strengthened concrete elements the bond behaviour at the end of the reinforcement can be assimilated to what happens in bond tests, thus assuming the interfacial shear

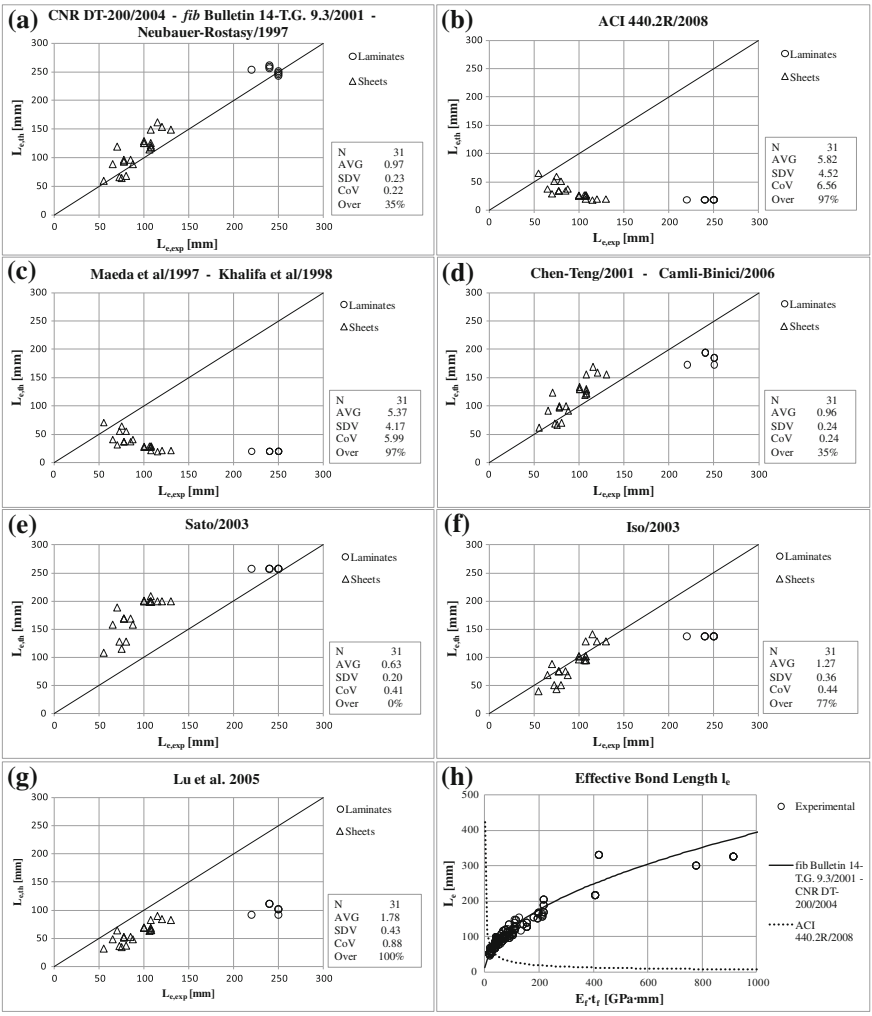

Fig. 3.26 Comparison between experimental and analytical effective bond length results **a**–**g**, and between experimental and analytical effective bond length as the FRP stiffness increases for the considered codes\recommendations **h**

stresses predominant and the normal ones negligible, the following well-known formulation for the maximum tensile load in the FRP reinforcement (Holzenkampfer 1994; Brosens and van Gemert 1999; Chen and Teng 2001; Teng and Yao 2007; CNR-DT 200 2004; Seracino et al. 2004a; Yao et al. 2005; Toutanji et al. 2007) is assumed:

$$F_{\max} = b_f \sqrt{2 \cdot E_f \cdot t_f \cdot \Gamma_f} \tag{3.66}$$

where b_f, t_f, E_f are width, thickness and Young's modulus of the external FRP reinforcement, and Γ_f is the fracture energy associated to the bond law of the FRP reinforcement-concrete interface. Such a general expression has been calibrated on results of pull-push bond tests and the fracture energy has been assumed depending on the compressive strength of concrete, as follows:

$$\Gamma_f = k_b^2 \cdot f_{cm}^{2/3} \tag{3.67}$$

Thus, the following formulations of the mean, f_{fbm}, and the characteristic debonding strength, f_{fbd}, in the FRP reinforcement are proposed:

$$f_{fbm} = k_m \cdot k_b \cdot \beta_L \cdot \sqrt{\frac{2 \cdot E_f}{t_f} \cdot f_{cm}^{2/3}} \text{ [forces in N, lengths in mm]} \tag{3.68}$$

$$f_{fbk} = k_k \cdot k_b \cdot \beta_L \cdot \sqrt{\frac{2 \cdot E_f}{t_f} \cdot f_{cm}^{2/3}} \text{ [forces in N, lengths in mm]} \tag{3.69}$$

where $k_m = 0.250$ and $k_{0.05} = 0.170$. The shape factor, k_b, and the length factor, β_L, are defined as:

$$k_b = \sqrt{\frac{2 - b_f/b_c}{1 + b_f/b_c}} \tag{3.70}$$

$$\beta_L = \frac{L_b}{L_e} \cdot \left(2 - \frac{L_b}{L_e}\right) < 1 \qquad \text{if } L_b < L_e \text{ and } \beta_L = 1 \text{ if } L_b > L_e \tag{3.71}$$

where L_b is the bonded length, b_c is the concrete section width, f_{cm} is the mean cylinder compressive strength of concrete.

The coefficient k_m has been assessed using the experimental results collected in more than 280 bond tests (Bilotta et al. 2011) on concrete elements externally bonded with FRP plates and sheets with compressive strength f_{cm} variable in the range 15–62 MPa, Young's modulus of FRP reinforcement 82÷400 GPa, thickness of FRP reinforcement 0.083÷1.6 mm, layers of strengthening 1÷3, reinforcement—to concrete width ratio 0.15÷1. In particular, k_m has been assessed by means of a statistical procedure as the least-square coefficient minimizing the difference between theoretical values and experimental results according to the design by testing philosophy to determine capacity models suggested in (see Chap. 2, CEN, 1993, Eurocode 0). The value $k_{0.05}$ has been then calculated under the hypothesis that the debonding load has a normal distribution.

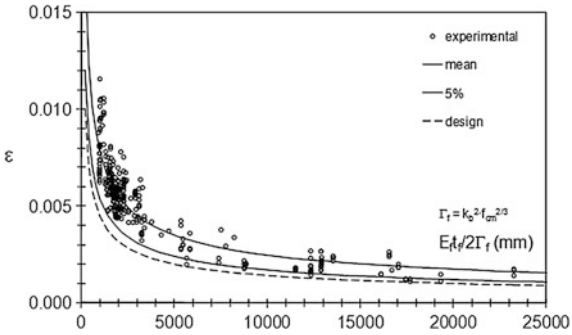

Fig. 3.27 Comparison of experimental and theoretical values of debonding strain according to Eqs. (3.3) and (3.4)

In Fig. 3.27 the distribution of experimental values of maximum strain at debonding collected by (Bilotta et al. 2011) is plotted in comparison with the mean and characteristic provisions given by Eqs. (3.68) and (3.69).

Associated to the bond model given by Eqs. (3.3) and (3.4), the effective bond length L_e may be estimated by the following expressions:

$$L_e = \frac{\pi}{k_b} \cdot \sqrt{\frac{E_f \cdot t_f}{8 \cdot f_{cm}^{2/3}}} \quad \text{for mean provision} \tag{3.72a}$$

$$L_e = 1.5 \cdot \frac{\pi}{k_b} \cdot \sqrt{\frac{E_f \cdot t_f}{8 \cdot f_{cm}^{2/3}}} \quad \text{for design provision} \tag{3.72b}$$

The failure mode indicated as "*Debonding at the end anchorage zone for Concrete Cover Delamination and Critical Diagonal Crack debonding*", is usually determined by a diagonal shear crack formed near the support end of the FRP reinforcement in the unstrengthened portion. When the distance between the FRP reinforcement end and the adjacent beam support is very small, the failure can be induced by the formation of a major shear crack intersecting the plate with the detachment of a thin layer of concrete or associated to the complete concrete cover delamination. In this case a real CDC debonding occurred due to the formation of the critical diagonal crack in the strengthened portion. If the plate end distance is increased, the CDC may fall outside the plated region, and only concrete cover separation is observed. In presence of internal steel stirrups, the shear crack can propagates below the steel stirrups and lead to the superficial debonding or to concrete cover delamination. On the contrary, the lack of internal steel shear reinforcement could induce the propagation of the diagonal crack along the height of the beam. This has been often observed in experimental bending tests where concentrated loading points are applied. Since the lacking of internal steel stirrups is

one of the cause of such failure, the behaviour can be significantly enhanced by shear strengthening measures, such as the use of externally bonded FRP U-shaped jackets, that can restrain the opening-up of the shear crack as well as the separation of the strengthening plate and the concrete cover. A variety of strength models have been proposed for calculating the strength for such a failure (Janzse 1997; Oehlers and Moran 1990; Smith and Teng 2002a; Oehlers et al. 2004; Gao et al. 2005; Teng and Yao 2007; Toutanji et al. 2006); most of them are based on shear verification or combined shear-moment verification at the end section of the FRP reinforcement. The failure load associated to the CDC debonding or to the concrete cover delamination should be range between the shear strength of the concrete in the unplated beam and the full shear strength of the plated beam.

For the "*Debonding at intermediate cracks due to shear stresses (IC Debonding)*", three possible approaches are proposed: a simplified approach, an approach based on the envelope line of tensile stress and an approach based on the force transfer between the concrete and external FRP reinforcement.

In the simplified approach, similarly to what reported in (CNR-DT 200 2004), at the ultimate limit state the maximum bending moment can be calculated assuming that in the FRP reinforcement the tensile stress does not exceed the bond strength given by the following relationship:

$$f_{fbm,IC} = k_{cr,m} \cdot f_{fbm} \tag{3.73a}$$

$$f_{fbm,IC} = k_{cr,m} \cdot f_{fbm} \tag{3.73b}$$

where the values of the bond strength at the end, f_{fbm} and f_{fbm}, are defined by Eqs. 3.3 and 3.4 and the coefficients $k_{cr,m}$ and $k_{cr,d}$ can be taken equal to 2.0 and 1.5, respectively, if specific data are not available.

The approach based on the envelope line of tensile stress can be complex for design purposes, since in most cases it requires the evaluation of the tensile stress in the FRP reinforcement in adjacent cracks and the definition of the crack spacing. According to this approach, indeed, the stress variation, $\Delta\sigma_f$, in the FRP strengthening between two subsequent cracks should not exceed a suitable limit value $\Delta\sigma_R$, which corresponds to the maximum increase in tensile stress that can be transferred by means of bond stresses along the cracks spacing. The value $\Delta\sigma_R$ depends, in general, on the bond constitutive law, the distance between cracks, s_r, and the stress level, σ_f, in the FRP reinforcement under the ultimate load condition (fib bulletin 14 2001; Teng et al. 2003; Wu and Niu 2007; Oller et al. 2009; DAfStb 2012).

To avoid the calculation of the tensile stress variation in adjacent cracks, $\Delta\sigma_f$, an alternative approach can be used (Oller et al. 2009). This approach consists of a bending-shear interaction diagram related to IC debonding, obtained through the limit stress variation $\Delta\sigma_R$. This multi-linear diagram is obtained through the shear and bending moment values associated to the maximum transferred force along the crack spacing for some key points related to steel yielding in the critical cracks

involved. This method directly compares the design shear force and bending moment values to the IC debonding interaction diagram, but the disadvantage of this method remains the evaluation of the crack spacing.

The approach based on the force transfer between concrete and FRP is simpler than the previous one and does not depend on the crack spacing. This approach implies the limitation of the interfacial shear stress resulting from the change of tensile force along the FRP reinforcement to a certain design shear strength.

References

Achintha, P. M. M., & Burgoyne, C. J. (2008). Fracture mechanics of plate debonding. *Journal of Composites for Construction, 12*(4), 396–404.

Achintha, P. M. M., & Burgoyne, C. J. (2011). Fracture mechanics of plate debonding: validation against experiment. *Construction and Building Materials, 25*(6), 2961–2971.

ACI (2002). *Design and construction of externally bonded FRP systems for strengthening concrete structures.* ACI 440.2R-02, American Concrete Institute, Farmington Hills, Mich.

ACI 440.2R-08 (2008). *Guide for the Design and Construction of Externally Bonded FRP Systems for Strengthening Concrete Structures*. ACI440.2R-08 American Concrete Institute, Farmington Hills, MI, 2008, 76 pp.

ACI Committee 440F (2002). *Guide for design and construction of externally bonded FRP systems for strengthening concrete structures*.

Adhikary, B. B., & Mutsuyoshi, H. (2001). Study on the bond between concrete and externally bonded CFRP sheet. In *Proceedings of the 6th International Symposium on Fiber Reinforced Polymer Reinforcement for Concrete Structures (FRPRCS-5)* (vol. 1, pp. 371–378).

Ahmed, O., van Gemert, D., & Vanderwalle, L. (2001). Improved model for plate end shear of CFRP strengthened RC beams. *Cement & Concrete Composites, 23*(1), 3–19.

Aiello, M.A., & Leone, M. (2005). Experimental bond analysis of concrete—FRP (fiber reinforced polymer) reinforced. In *Proceedings of fib Symposium "Keep Concrete Attractive*". Budapest, Hungary, May.

Alam, M. S., Kanakubo, T., & Yasojima, A. (2012). Shear-peeling bond strength between continuous fiber sheet and concrete. *ACI Structural Journal, 109*(1), 75–82.

Ali-Ahmad, M., Subramaniam, K. V., & Ghosn, M. (2006). Experimental investigation and fracture analysis of bebonding between concrete and FRP. *Journal of Engineering Mechanics, 132*(9), 914–923.

Ali-Ahmad, M., Subramaniam, K. V., & Ghosn, M. (2007). Analysis of scaling and instability in FRP-concrete shear debonding for beam-strengthening applications. *Journal of Engineering Mechanics, 133*(1), 58–67.

Anderson, T. L. (2004). *Fracture mechanics: fundamentals and applications*. Boca Raton: Florida, CRC Press.

Bazant, Z. P., & Planas, J. (1997). *Fracture and size effect in concrete and other quasibrittle materials*. Boca Raton: Florida, CRC Press.

Bilotta, A. (2010). *Behaviour of FRP-to-concrete interface: theoretical models and experimental results*, *Doctoral thesis, Naples*. Italy: University of Naples "Federico II".

Bilotta, A., Ceroni, F., Nigro, E., & Pecce M. (2011b). Design by testing of debonding load in RC element strengthened with EBR FRP materials. *10th International Symposium on Fiber Reinforced Polymer Reinforcement for Reinforced Concrete Structures*,*Tampa, Florida, USA.* April 2-4, 2011.

Bilotta, A., Ceroni, F., Nigro, E., Di Ludovico, M., Pecce, M., & Manfredi, G. (2011a). Bond efficiency of EBR and NSM FRP systems for strengthening of concrete members. Journal of

Composites for Construction, ASCE. 15(5), 757–772. October 1, 2011, ISSN 1090-0268/2011/5.

Bilotta, A., Faella, C., Martinelli, E., & Nigro, E. (2011c). Indirect identification method for bilinear bond-law relationship, J. of Composites for Construction, ASCE, doi:10.1061/(ASCE)CC.1943-5614.0000253).

Bilotta, A., Faella, C., Martinelli, E., & Nigro, E. (2012). Indirect identification method of bilinear interface laws for FRP bonded on a concrete substrate. *Journal of Composites for Construction*, 16, 171–184, ISSN: 1090-0268, doi:10.1061/(ASCE)CC.1943-5614.0000253.

Bizindavyi, L., & Neale, K. W. (1999). Transfer lengths and bond strengths for composites bonded to concrete Journal of Composites for Construction ASCE n. 153–160.

Bizindavyi, L., Neale, K. W., & Erki, M. A. (2003). Experimental Investigation of Bonded Fiber Reinforced Polymer-Concrete Joints under Cyclic Loading. *Journal of Composites for Construction ASCE, 7*(2), 127–134.

Blontrock, H., Taerwe, L., & Vanwalleghem, H. (2002). Bond testing of externally glued FRP laminates at elevated temperature. In *Proceedings of the International Symposium Bond in Concrete: from research to standards*, *Budapest* (pp. 648–654). ISBN 963-420-714-6.

Boschetto, G., Pellegrino, C., Tinazzi, D., & Modena, C. (2006). Bond behaviour between FRP sheets and concrete: an experimental study. In *Proceedings of the 2nd International Fib Congress. June, Naples, Italy*, CDROM.

Brosens, K. (2001). *Anchorage of externally bonded steel plates and CFRP laminates for the strengthening of concrete elements*. PhD thesis, K.U. Leuven, 2001, 225 pp.

Brosens, K., & van Gemert, D. (1997). Anchoring stresses between concrete and carbon fibre reinforced laminates. In *Proceedings. of the 3rd International Symposium on Non-Metallic (FRP) Reinforcement for Concrete Structures*, Japan Concrete Institute, Sapporo, 1, 271–278.

Buyukozturk, O., Gunes, O., & Karaca, E. (2004). Progress on under-standing debonding problems in reinforced concrete and steel members strengthened using FRP composites—Short survey. *Con-struction and Building Materials, 18*(1), 9–19.

Camli, U. S., & Binici, B. (2007). Strength of carbon fiber reinforTced polymers bonded to concrete and masonry. *Construction and Building Materials, 21*, 1431–1446.

Carloni, C., & Subramaniam, K. V. (2010). Direct determination of cohesive stress transfer during debonding of FRP from concrete. *Composite Structures, 93*(1), 184–192.

Carloni, C., & Subramaniam, K. V. (2012). Application of fracture mechanics to debonding of FRP from RC members. *ACI SP 286-10*.

Carloni, C., & Subramaniam, K. (2013). Investigation of sub-critical fatigue crack growth in FRP/concrete cohesive interface using digital image analysis. *Compos—Part B: Eng, 51*, 35–43.

Carloni, C., Subramaniam, K. V., Savoia, M., & Mazzotti, C. (2012). Experimental determination of FRP-concrete cohesive interface properties under fatigue loading. *Composite Structures, 94*, 1288–1296.

Carrara, P., Ferreti, D., Freddi, F., & Rosati, G. (2011). Shear tests of carbon fiber plates bonded to concrete with control of snap-back. *Engineering Fracture Mechanics, 79*, 2663–2678.

Carrara, P., & Ferretti, D. (2013). A finite-difference model with mixed interface laws for shear tests of FRP plates bonded to concrete. *Composites: Part B, 54*, 329–342.

Ceroni, F., Garofano, A., & Pecce, M. (2014). Modelling of bond behavior in masonry elements externally bonded with FRP materials, in press on Composite part B, Elsevier.

Ceroni, F., & Pecce, M. (2002). Bond behaviour of R.C. elements externally reinforced with FRP laminates. In *Proceedings of the International Symposium Bond in Concrete—from research to standards. Budapest* (pp. 622-629) ISBN 963-420-714-6.

Ceroni, F., & Pecce, M. (2005). Strength and ductility of RC beams strengthened with FRP sheets under monotonic and cyclic loads. *Proceedings. of fib Symposium "Keep concrete Attractive", Budapest, Hungary* (418–423).

Ceroni, F., & Pecce, M. (2006). Bond tests on concrete and masonry blocks externally bonded with CFRP. In *Proceedings of Third International Conference on FRP Composites in Civil Engineering, CICE 2006*, Miami, Florida, USA, pp. 17–20.

Ceroni, F., & Pecce, M. (2007). Bond performance in concrete elements strengthened with CFRP sheets. In *Proceedings of FRP RCS8*, July, Patrasso, Greece, CD ROM.

Ceroni, F., & Pecce, M. (2010). Evaluation of bond Strength in concrete element externally reinforced with CFRP sheets and anchoring devices. *Journal of Composites for Construction, ASCE, 14*(5), 521–530.

Ceroni, F., Pecce, M., Matthys, S., & Taerwe, L. (2008). "Bond tests on concrete elements with CFRP and anchorage systems", *Composites: Part B. Elsevier, 39*, 429–441.

Chajes, M. J., Finch, W. W., Januszka, T. F., & Thomson, T. A. (1996). Bond and force transfer of composite material plates bonded to concrete. *ACI Structural Journal*, 93(2), 208–217.

Chen, J. F., & Teng, J. G. (2001). Anchorage strength models for FRP and Steel Plates bonded to concrete. *ASCE J. of Structural Engineering, 127*(7), 784–791.

Chen, J. F., & Teng, J. G. (2003) Shear capacity of FRP-strengthened RC beams: FRP debonding. *Construction and Building Materials*, *17*, 27–41.

Chen, J. F., Yang, Z. J., & Holt, G. D. (2001). FRP or steel plate-to-concrete bonded joints: effect of test methods on experimental bond strength. *Steel Compos Structures, 1*(2), 231–244.

CNR-DT 200. (2004). Instructions for design, execution and control of strengthening interventions through fiber-reinforced composites, Council of National Research, Rome.

CNR. (2013). Guide for the design and construction of externally bonded FRP systems for strengthening existing structures, CNR-DT 200 R1/2013, National Research Council.

Coronado, C. A., & Lopez, M. M. (2005). Modelling of FRP-concrete bond using nonlinear damage mechanics. In C. K. Shield & J. P. Busel(Eds.), *Proceedings of 7th International Symposium on FRP Reinforcement for Concrete Structures*, Kansas City, Missouri.

Cruz, J. M. S., & Barros, J. A. O. (2002). Bond behaviour of carbon laminate strips into concrete by pullout bending test. In *Proceedings of the International Symposium "Bond in Concrete—from research to standards", Budapest* (pp. 614–621). ISBN 963-420-714-6.

DAfStb. (2012). On the strengthening of concrete parts with adhesively bonded reinforcement, German Committee for Reinforced Concrete.

Dai, J. G., Sato, Y., Ueda, T., & Sato, Y. (2005b). Static and Fatigue Bond Characteristics of Interfaces between CFRP Sheets and Frost Damage Experienced Concrete. In *Proceedings of FRPRCS-7*, (pp. 1515–1530) ACI-SP-230-86.

Dai, J., Ueda, T., Hiroki, O., & Sato, Y. (2003). Experimental study on the mix-mode fracture of FRP sheet-concrete interface. *JCI International Symposium on Latest Achievement in Technology and Research on Retrofitting Concrete Structures, Interface Mechanics and Structural Performance*, *Kyoto, Japan* (pp. 121–128).

Dai, J., Ueda, T., & Sato, Y. (2005a). Development of the nonlinear bond stress–slip model of fiber reinforced plastics sheet-concrete interfaces with a simple method. *Journal of Composites for Construction, ASCE* 9(1), 52–62.

Dai, J. G., Ueda, T., & Sato, Y. (2006). Unified analytical approaches for determining shear bond characteristics of FRP-concrete interfaces through pullout tests. *Journal of Advanced Concrete Technology, 4*, 133–145.

Davalos, J. F., Kodkani, S. S., & Ray, I. (2006). Fracture mechanics method for Mode-I interface evaluation of FRP bonded to concrete substrates. *Journal of Materials in Civil Engineering, 18* (5), 732–742.

De Lorenzis, L., Miller, B., & Nanni, A. (2001). Bond of Fiber-Reinforced Polymer Laminates to Concrete. ACI Materials Journal. 98-M29, 256–264.

Delaney, J., & Karbhari, V. (2007). Defect criticality in FRP strengthening. In *Proceedings of the 8th International Symposium in Fiber-Reinforced (FRP) Polymer Reinforcement for Concrete Structures (FRPRCS-8) CD-ROM*, *University of Patras, Greece* (pp. 3–20).

Diab, H., Wu, Z., & Iwashita, K. (2007). Experimental and numerical investigation of fatigue behavior of frp-concrete interface. In *Proceeding of FRPRCS-8*, *Patras, Greece* (pp. 16–18).

Dimande, A. O., Juvenades, L. F. P., & Figueiras, J. A. (2005). Bond characterization between concrete and fiber-reinforced polymer. In *Proceedings of 3*rd *International Conference on Composites in Construction, CCC2005*, *Lyon, France*.

Elices, M., Guinea, G. V., Gómez, J., & Planas, J. (2002). The cohesive zone model: advantages, limitations and challenges. *Engineering Fracture Mechanics, 64*, 137–163.

Faella, C., Martinelli, E., & Nigro, E. (2002). Aderenza tra calcestruzzo e fogli di FRP utilizzati come placcaggio di elementi inflessi. Parte II: modelli teorici ed elaborazioni numeriche. Atti del XIV Congresso C.T.E., Bologna.

Faella, C., Martinelli, E., & Nigro, E. (2003). Interface behaviour in FRP plates bonded to concrete: experimental tests and theoretical analyses. In *Proceedings of the International Conference on Advanced Materials for Construction of Bridges, Buildings and other Structures—III, Davos (Svizzera)*, 7–12 September 2003.

Faella, C., Martinelli, E., & Nigro, E (2006a). Formulation and Validation of a Theoretical Model for Intermediate Debonding in FRP Strengthened RC Beams. In *Proceedings of the 2nd International fib Congress, Naples, Italy*, 5–8 June 2006, Paper 0735.

Faella, C., Martinelli, E., & Nigro, E (2006b). Intermediate Debonding in FRP Strengthened RC Beams: A Parametric Analysis, In *Proceedings of the 2nd International fib Congress, Naples, Italy*, 5–8 June 2006, Paper 0993.

Faella, C., Martinelli, E., & Nigro, E., (2007a). Direct versus Indirect identification of FRP-to-concrete interface relationships, Asia-Pacific Conference on FRP in Structures. Hong Kong (China), 12–14 December 2007.

Faella, C., Martinelli, E., & Nigro, E. (2008a). Formulation and Validation of a Theoretical Model for Intermediate Debonding in FRP Strengthened RC Beams. *Composites Part B*, 39(4), 645–655. ISSN 1359-8368.

Faella, C., Martinelli, E., & Nigro, E. (2009). Direct versus Indirect Method for Identifying FRP-to-Concrete Interface Relationships. *ASCE Journal for Composites for Construction*, 13 (3), 226–233. ISSN 1090-0268.

Fanning, P. J., & Kelly, O. (2001). Ultimate response of RC beams strengthened with CFRP plates. *Journal of Composites for Construction, ASCE, 5*(2), 122–127.

Ferracuti, B., Savoia, M., & Mazzotti, C. (2006). A numerical model for FRP-concrete delamination. *Composites: Part B, 37*, 356–364.

Ferracuti, B., Savoia, M., & Mazzotti, C. (2007). Interface law for FRP-concrete delamination. *Composite Structures, 80*(4), 523–531.

fib. (2001). Externally Bonded FRP Reinforcement for RC Structures. fib Bulletin 14, Technical Report, Task Group 9.3—FRP Reinforcement for Concrete Structures, International Federation for Structural Concrete, Lausanne (CH). ISBN 978-2-88394-054-3.

Focacci, F., Nanni, A., & Bakis, C. E. (2000). Local bond-slip relationship for FRP reinforcement in concrete. *Journal of Composites for Construction, 4*(1), 24–31.

Garden, H. N., & Hollaway, L. C. (1998). An experimental study of the influence of plate end anchorage of carbon fibre composite plates used to strengthen reinforced concrete beams. *Composite Structures, 42*, 175–188.

Guadagnini, M., Serbescu, A., Palmieri, A., Matthys, S, Bilotta, A, Nigro, E, Ceroni, F, Czaderski, C, Olia, S, Szambo, Z, Balazs, G, & Mazzotti, C. (2012). Round robin test on the bond behaviour of externally bonded frp systems to concrete. In *Proceedings of CICE 2012, 6th International Conference on FRP Composites in Civil Engineering*, *Rome, Italy*, *CD ROM* (pp. 13–15).

Gunes, O. (2004), *A Fracture based approach to understanding debonding in FRP bonded structural members*, PhD Thesis, Massachusetts Institute of Technology, Cambridge, MA.

Gunes, O., Buyukozturk, O., & Karaca, E. (2009). A Fracture-based model for FRP debonding in strengthened beams. *Engineering Fracture Mechanics, 76*, 1897–1909.

Guo, Z. G., Cao, S. Y., Sun, W. M., & Lin X. Y. (2005). Experimental study on bond stresses-slip behaviour between FRP sheets and concrete. In Chen & Teng (Eds.), *Proceedings of the International Symposium on Bond Behaviour of FRP in Structures, BBFS 2005* (pp. 77–83).

Hearing, B. F. (2000), *Delamination of reinforced concrete retrofitted with fiber reinforced plastics*, PhD Thesis, Massachusetts Institute of Technology, Cambridge, MA.

Hillerborg, A., Modéer, M., & Petersson, P. E. (1976). Analysis of crack formation and crack growth in concrete by means of fracture mechanics and finite elements. *Cement and Concrete Research, 6*, 773–782.

Hiroyuki, Y., & Wu, Z. (1997). Analysis of debonding fracture properties of CFS strengthened member subject to tension. In *Proceedings of 3rd international symposium on non-metallic (FRP) reinforcement for concrete structures* (vol. 1, pp. 284–94).

Holzenkaempfer. (1994). Ingenieurmodelle des verbundes geklebter bewehrung fur betonbauteile, Dissertation, TU Braunschweig (in German).

Horiguchi, T., & Saeki, N. (1997). Effect of test methods and quality of concrete on bond strength of CFRP sheet. In *Proceedings of International Symposium on Non-metallic (FRP) reinforcement for concrete structures*, Sapporo, Japan, Japan Concrete Institute, Vol.1, pp. 265–270.

Hutchinson, J. W., & Suo, Z. (1992). Mixed-mode cracking in layered materials. *Advances in Applied Mechanics, 29*, 63–191.

International Concrete Repair Institute. (1997). Selecting and Specifying Concrete Surface Preparation for Sealers, Coatings and Polymer Overlays. Technical Guideline 1997 No. 03732.

Iovinella, I., Prota, A., & Mazzotti, C. (2013). Influence of surface roughness on the bond of FRP laminates to concrete, *Construction and Building Materials*, *40*, 533–542.

Japan Concrete Institute (JCI). (2003). Technical report of technical committee on retrofit technology. In *Proceedings International Symposium on Latest Achievement of Technology and Research on Retrofitting Concrete Structures*.

Khalifa, A., Gold, W. J., Nanni, A., & Aziz, A. (1998). Contribution of externally bonded FRP to shear capacity of RC flexural members. *Journal of Composites for Construction, ASCE, 2*(4), 195–203.

Ko, H., & Sato, Y. (2007). Bond stress-slip relationship between FRP sheet and concrete under cyclic load. *Journal of Composites for Construction ASCE, 11*(4), 419–426.

Kobayashi, A., Matsui, S., & Kishimoto, M. (2003). Fatigue Bond of Carbon Fiber Sheets and Concrete in RC Slabs Strengthened by CFRP. In K.H. Tan (Ed.), *Proceedings of FRPRCS-6* (vol. 2, pp. 865–874).

Leone, M., Aiello, M. A., & Matthys, S. (2006). The influence of service temperature on bond between FRP reinforcement and concrete. In *Proceedings of the 2nd International Fib Congress*, *Naples, Italy*.

Liu, K., & Wu, Y. F. (2012). Analytical identification of bond-slip relationship of EB-FRP joints. *Composite; Part B, 43*, 1955–1963.

Lu, X. Z., Teng, J. G., Ye, L. P., & Jiang, J. J. (2005). Bond–slip models for FRP sheets/plates bonded to concrete. *Engineering Strucures*, *27*, 920–937.

Maeda, T., Asano, Y., Sato, Y., Ueda, T., & Kakuto, Y. (1997). A study on bond mechanism of carbon fiber sheet. In *Proceedings of the 3rd International Symposium on Non-Metallic (FRP) Reinforcement of Concrete Structures*, Vol. 1, October.

Malek, A. M., Saadatmanesh, H., & Ehsani, M. R. (1998). Prediction of failure load of R/C beams strengthened with FRP plate due to stress concentration at the plate end. *ACI Structural Journal* 95(2), 142–152. ISSN 1090-0268.

Martinelli, E., Czaderski, C., & Motavalli, M. (2011). Modeling in-plane and-of-plane displacement fields in pull-off tests FRP strips. *Engineering Structures, 33*, 3715–3725.

Matana, M., Nanni, A., Dharani, L., Silva, P., & Tunis, G. (2005). Bond performance of steel reinforced polymer and steel reinforced grout. In *Proceedings of the International Symposium on Bond Behaviour of FRP in structures*, *Honk Kong* (pp. 125–132).

Mazzotti, C., Ceroni, F., & Pecce, M., (2013). Effect of test set-up of bond strength in concrete elements externally bonded with CFRP plates. In J. Barros & J. Sena-Cruz (Eds.), *Proceedings of FRPRCS11, UM, Guimarães*.

Mazzotti, C., Savoia, M., & Ferracuti, B. (2005). A New Set-Up for FRP-Concrete Stable Delamination Test. In C. K. Shield & J. P. Busel (Ed.), *Proceedings of 7th International Symposium FRP Reinforcement for Concrete Structures*, *Kansas City, Missouri* (pp. 165–180).

Mazzotti, C., Savoia, M., & Ferracuti, B. (2007). Mode II fracture energy and interface law for FRP—concrete bonding with different concrete surface preparations. In *Proceedings of FRAMCOS 6. FRAMCOS 6—Fracture Mechanics of Concrete and Concrete Structures. Catania, Italy*. (vol. 2, pp. 1249–1257).

Mazzotti, C., Savoia, M., & Ferracuti, B. (2008). An experimental study on delamination of FRP plates bonded to concrete. *Construction and Building Materials, 22*, 1409–1421.

Mazzucco, G., Salomoni, V. A., & Majorana, C. E. (2012). Three-dimensional contact-damage coupled modeling of FRP reinforcements—simulation of the delamination and long term process. *Computer and Structures, 110–111*, 15–31.

McSweeney, B. M., & Lopez, M. M. (2005). FRP-Concrete Bond Behavior: A Parametric Study Through Pull-Off Testing. In C. K. Shield & J. P. Busel (Eds.), *Proceedings of the 7th International Symposium FRP Reinforcement for Concrete Structures, Kansas City, Missouri* (pp. 441–460).

Miller, B., & Nanni, A. (1999). Bond Between CFRP Sheets and Concrete Congress. In *Proceedings ASCE 5th Materials Cincinnati, Ohio* (pp. 240–247).

Nakaba, K., Kanakubo, T., Furuta, T., & Yoshizawa, H. (2001). Bond behaviour between fiber-reinforced polymer laminates and concrete. *ACI Structural Journal, 98*(3), 359–367.

Neubauer, U., & Rostásy, F. S. (1997). Design aspects of concrete structures strengthened with externally bonded CFRP-plates. In *Proceedings of 7th International Conference on Structural Faults and Repair Concrete + Composites* (vol. 2, pp. 109–118).

Nigro, E., Di Ludovico, M., & Bilotta, A. (2008). Concrete interface relationships under monotonic and cyclic actions. In *Fourth International Conference on FRP Composites in Civil Engineering (CICE2008)*, *Zurich, Switzerland* (pp. 22–24).

Nigro, E., Di Ludovico, M., & Bilotta, A. (2011). Experimental Investigation of FRP-Concrete Debonding under Cyclic Actions. *Journal Of Materials In Civil Engineering*, 23, 360–371. ISSN: 0899-1561, doi:10.1061/(ASCE)MT.1943-5533.0000173.

Nguyen, D. M., Chan, T. K., & Cheong, H. K. (2001). Brittle failure and bond development length of CFRP–concrete beams. *Journal of Composites for Construction*, *ASCE*, *5*(1), 12–17.

Oehlers, D. J., & Moran, J. P. (1990). Premature failure of externally plated reinforced-concrete beams. *Journal of Structural Engineering—ASCE* 116(4), 978–995. ISSN 0733-9445.

Oller, E., Cobo Del Arco, D., & Marì Bernat, A. R. (2009). Design proposal to avoid peeling failure in FRP-strengthened reinforced concrete beams. *Journal of Composites for Construction*, *13*(5), 384–393.

Pellegrino, C., & Modena, C. (2009). Influence of axial rigidity on FRP-concrete bond behavior: an analytical study. *Advances in Structural Engineering, 12*(5), 639–649.

Pellegrino, C., Tinazzi, D., & Modena, C. (2008). Experimental study on bond behavior between concrete and FRP reinforcement. *Journal of Composites for Construction, ASCE* 12(2), 180–189.

Pham, H., & Al-Mahaidi, R. (2004). Prediction models for debonding failure loads of CFRP retrofitted RC beams. In *Proceedings of the 2nd International Conference on FRP Composites in Civil Engineering, CICE 2004, Adelaide (Australia)* (pp. 8–10), December 2004.

Pham, H. B., & Al-Mahaidi, R. (2005). Modelling of CFRP—concrete shear-lap tests. In *Proceedings of 3rd International Conference on Composites in Construction, CCC2005*, *Lyon, France*.

Rabinovitch, O. (2004). Fracture mechanics failure criteria for RC beams strengthened with FRP strips—a simplified approach. *Composite Structures, 64*, 479–492.

Rabinovitch, O. (2008). Debonding analysis of fiber-reinforced-polymer strengthened beams: cohesive zone modeling versus a linear elastic fracture mechanics approach. *Engineering Fracture Mechanics, 75*, 2842–2859.

Rabinovitch, O. (2012). Dynamic debonding on concrete beams strengthened with composite materials. *International Journal of Solids and Structures, 49*, 3641–3658.

Rahimi, H., & Hutchinson, A. (2001). Concrete beams strengthened with externally bonded FRP plates. *Journal of Composites for Construction, ASCE, 5*(1), 44–56.

Roberts, T. M. (1989). Approximate analysis of shear and normal stress concentrations in the adhesive layer of plated RC beams, The Structural Engineer, 67(12), 1989. *ISSN, 229–233*, 0039–2553.

Said, & Wu. (2008). Evaluating and proposing models of predicting IC Debonding Failure. *ASCE Journal of Composites for Construction* 12(3), 284—299. June 1, 2008.

Savoia, M., Bilotta, A., Ceroni, F., Di Ludovico, M., Fava, G., Ferracuti, B., Mazzotti, C., Nigro, E., Olivito, R., Pecce, M., & Poggi, C. (2009). Experimental round robin test on FRP concrete bonding. In *Proceedings of FRP RCS9, Sydney, Australia* (pp. 13–15).

Savoia, M., Ferracuti, B., & Mazzotti, C. (2003). Non linear bond-slip law for FRP-concrete interface. In *Proceedings of the conference FRPRCS-6, Singapore*.

Serbescu, A., Guadagnini, M., & Pilakoutas, K. (2013). Standardised double-shear test for determining bond of FRP to concrete and corresponding model development. *Composites Part B Engineering, 55*, 277–297.

Shen, X., Myers, J. J., Maerz, N., & Galecki, G. (2002). Effect of surface roughness on the bond performance between FRP laminates and concrete. In B. Benmokrane, & E. El-Salakawy (Eds.), *Proceedings of the 2nd International Conference on Durability of Fiber Reinforced Polymer (FRP) Composites for Construction*, *University of Sherbrooke, Canada* (pp. 607–616).

Smith, S. T., & Teng, J. G. (2002). FRP-strengthened RC beams-II: assessment of debonding strength models. *Engineering Structures, 24*(4), 397–417.

Subramaniam, K. V., Carloni, C., & Nobile, L. (2007). Width effect in the interface fracture during shear debonding of FRP sheets from concrete. *Engineering Fracture Mechanics, 74*(4), 578–594.

Subramaniam, K. V., Carloni, C., & Nobile, L. (2011). An understanding of the width effect in FRP–concrete debonding. *Strain, 47*, 127–137.

Sutton, M. A., Orteu, J. J., & Shreier, H. W. (2009). *Image correlation for shape, motion and deformation measurements*. New York: Springer.

Sutton, M. A., Wolters, W. J., Peters, W. H., Ranson, W. F., & McNeill, S. R. (1983). Determination of displacements using an improved digital correlation method. *Image and Vision Computing, 1*(3), 133–139.

Takeo, K., Matsushita, H., Makizumi, T., & Nagashima, G. (1997). Bond characteristics of CFRP sheets in the CFRP bonding technique. In *Proceedings of Japan Concrete Institute* (Vol. 19, No. 2, pp. 1599–1604).

Taljsten, B. (1996). Strengthening of concrete prisms using the plate-bonding technique. *International Journal of Fracture, 82*, 253–266.

Taljsten, B. (1997a). Strengthening of beams by plate bonding. *ASCE Journal of Materials in Civil Engineering* 9(4), 206–211. ISSN 1943-5533.

Taljsten, B. (1997b) Defining anchor lengths of steel and CFRP plates bonded to concrete. *International Journal of Adhesion and Adhesives* 7(4), 319–327.

Teng, J. G., et al. (2001). FRP composites in civil engineering. Hong Kong: Elsevier.

Teng, J. G., Chen, J. F., Smith, S. T., & Lam, L. (2002). FRP Strengthened RC Structures, John Wiley & Sons Ltd., Chichester (UK), 245 pp. ISBN 0-471-48706-6.

Teng, J. G., Lu, X. Z., Ye, L. P., & Jiang, J. J. (2004). Recent Research on Intermediate Crack Induced Debonding in FRP Strengthened Beams. In *Proceedings of the 4th International Conference on Advanced Composite Materials for Bridges and Structures, Calgary, AB, Canada*.

Teng, J. G., Smith, S. T., Yao, J., & Chen, J. F. (2003). Intermediate crack-induced debonding in RC beams and slabs. *Construction and Building Materials* 17(6–7), 447–462. ISSN 0950-0618.

Teng, J. G., & Yao, J. (2007). Plate end debonding in FRP-plated RC beams-II: Strength model. *Engineering Structures, 29*, 2472–2486.

Tounsi, A., Hassaine, Daouadji T., Benyoucef, S., & Addabedia, E. A. (2009). Interfacial stresses in FRP-plated RC beams: Effect of adherend shear deformations, International Journal of Adhesion & Adhesives—Elsevier, 29(4), 2009. *ISSN, 343–351*, 0143–7496.

Toutanji, H., Saxena, P., Zhao, L., & Ooi, T. (2007). Prediction of interfacial bond failure of FRP —Concrete surface. *Journal of Composites for Construction, ASCE, 11*(4), 427–436.

Travassos, N., Ripper, T., & Appleton, J. (2005). Bond stresses characterization on CFRP-RC interfaces. In *Proceedings of 3rd International Conference Composites in Construction*, CCC2005, Lyon, France, July.

Ueda, T., & Dai, J. (2005). Interface Bond between FRP Sheets and Concrete Substrates: properties, numerical modeling and roles in member behavior. *Progress in Structural Engineering and Materials, John Wiley & Sons Ltd, 7*(1), 27–43.

Ueda, T., Sato, Y., & Asano, Y. (1999). Experimental study on bond strength of continuous carbon fiber sheet. In *Proceedings of 4th International Symposium on Fiber Reinforced Polymer reinforcement for Reinforced Concrete structure* (pp. 407–16).

Van Gemert, D. (1980). Force transfer in epoxy-bonded steel–concrete joints. *International Journal of Adhesion and Adhesives, 1*, 67–72.

Wan, B., Sutton, M. A., Petrou, M. F., Harries, K. A., & Li, N. (2004). Investigation of bond between fiber reinforced polymer and concrete undergoing global mixed mode I/II loading. *Journal of Engineering Mechanics, 130*(12), 1467–1475.

Wang, R. G., Liu, W. B., Dai, C. Q., Zhang, C. H., & Zhu, X. (2005). Study on adhesion properties of adhesive materials used for carbon fiber reinforced concrete structure. In *Proceedings of 3rd International Conference on Composites in Construction, CCC2005*, Lyon, France.

Wu, Z. S., & Niu, H. (2007). Prediction of crack-induced debonding failure in R/C structures flexurally strengthened with externally bonded FRP composites. *Doboku Gakkai Ronbunshuu E, 63*(4), 620–639.

Wu, Y. F., Xu, X. S., Sun, J. B., & Jiang, C. (2012). Analytical solution for the bond strength of externally bonded reinforcement. *Composite Structures, 94*, 3232–3939.

Wu, Z., & Yin, J. (2003). Fracturing behaviors of FRP-strengthened concrete structures. *Engineering Fracture Mechanics, 70*(10), 1339–1355.

Wu, Z. S., Yuan, H., & Niu, H. (2002). Stress transfer and fracture propagation in different kinds of adhesive joints. *Journal of Engineering Mechanics, 128*(5), 562–573.

Wu, Z. S., Yuan, H., Yoshizawa, H., & Kanakubo, T. (2001).Experimental/analytical study on interfacial fracture energy and fracture propagation along FRP-concrete interface. *ACI International SP-201-8,* 133–52.

Yao, J., Teng, J. G., & Chen, J. F. (2005). Experimental study on FRP-to-concrete bonded joints. *Composites Part B Engineering, 36*, 99–113.

Yi, W. H., Kang, D. E., Woo, H. S., Choi, K. S., Yoo, Y. C., & Keung-Hwan, K. (2006). A study on bond mechanism of fiber reinforced polymer bonded to concrete. *Proceeding of the 2nd International fib Congress*, *June, Naples, Italy, CDROM.*

Yuan, H., Teng, J. G., Seracino, R., Wu, Z. S., & Yao, J. (2004). Full-range behavior of FRP-to-concrete bonded joints. *Engineering Structures, 26*(5), 553–564.

Yuan, H., Wu, Z., & Yoshizawa, H. (2001). Theoretical solutions on interfacial stress transfer of externally bonded stee/composite laminates. *Structural Engineering/ Earthquake Engineering, 18*(1), 27–39.

Zhao, H. D., Zhang, Y., & Zhao, M. (2000). Research on the bond performance between CFRP plate and concrete. In *Proceedings of 1st Conference on FRP concrete structures of China* (pp. 247–53).

Zhou, Y. W., Wu, Y. F., & Yun, Y. (2010). Analytical modeling of the bond-slip relationship at FRP-concrete interfaces for adhesively-bonded joints. *Composites: Part B, 41*, 423–433.